



THE UNIVERSITY *of* EDINBURGH

Edinburgh Research Explorer

Fibroblast growth factors (FGFs) prime the limb specific *Shh* enhancer for chromatin changes that balance histone acetylation mediated by E26 transformation-specific (ETS) factors

Citation for published version:

Peluso, S, Douglas, A, Hill, A, De Angelis, C, Moore, BL, Grimes, G, Petrovich, G, Essafi, A & Hill, RE 2017, 'Fibroblast growth factors (FGFs) prime the limb specific *Shh* enhancer for chromatin changes that balance histone acetylation mediated by E26 transformation-specific (ETS) factors', *eLIFE*, vol. 6, e28590. <https://doi.org/10.7554/eLife.28590>

Digital Object Identifier (DOI):

[10.7554/eLife.28590](https://doi.org/10.7554/eLife.28590)

Link:

[Link to publication record in Edinburgh Research Explorer](#)

Document Version:

Peer reviewed version

Published In:

eLIFE

General rights

Copyright for the publications made accessible via the Edinburgh Research Explorer is retained by the author(s) and / or other copyright owners and it is a condition of accessing these publications that users recognise and abide by the legal requirements associated with these rights.

Take down policy

The University of Edinburgh has made every reasonable effort to ensure that Edinburgh Research Explorer content complies with UK legislation. If you believe that the public display of this file breaches copyright please contact openaccess@ed.ac.uk providing details, and we will remove access to the work immediately and investigate your claim.



1
2
3
4
5
6
7
8
9
10
11
12
13
14
15
16
17
18
19
20
21
22
23
24
25
26
27
28

Fibroblast growth factors (FGFs) prime the limb specific *Shh* enhancer for chromatin changes that balance histone acetylation mediated by E26 transformation-specific (ETS) factors

Silvia Peluso¹, Adam Douglas¹, Alison Hill¹, Carlo DeAngelis¹, Ben Moore¹, Graeme Grimes¹,
Giulia Petrovich¹, Abdelkader Essafi² and Robert E Hill^{1,3}

¹MRC-Human Genetics Unit, Institute of Genetics and Molecular Medicine, University of Edinburgh, Edinburgh UK EH4 2XU;

²School of Cellular and Molecular Medicine, Faculty of Biomedical Sciences, University of Bristol, University Walk, Bristol UK BS8 1TD

³Corresponding author-

Robert E Hill
MRC-Human Genetics Unit
MRC Institute of Genetics and Molecular Medicine
University of Edinburgh
Edinburgh UK EH4 2XU
Email: bob.hill@igmm.ed.ac.uk
Phone: +44-131-651-8621

29 **ABSTRACT**

30 Sonic hedgehog (*Shh*) expression in the limb bud organizing center called the ZPA is
31 regulated by the ZRS enhancer. Here, we examine in mouse and in a mouse limb-derived
32 cell line the dynamic events that activate and restrict the spatial activity of the ZRS. FGF
33 signalling in the distal limb primes the ZRS at early embryonic stages maintaining a poised,
34 but inactive state broadly across the distal limb mesenchyme. The ETS transcription factor,
35 ETV4, which is induced by FGF signalling and acts as a repressor of ZRS activity, interacts
36 with the histone deacetylase HDAC2 and ensures that the poised ZRS remains
37 transcriptionally inactive. Conversely, GABP α , an activator of the ZRS, recruits p300, which is
38 associated with histone acetylation (H3K27ac) indicative of an active enhancer. Hence, the
39 primed but inactive state of the ZRS is induced by FGF signalling and in combination with
40 balanced histone modification events establishes the restricted, active enhancer responsible
41 for patterning the limb bud during development.

42 **Key words**

43 Enhancer, ZRS, Shh, FGF, ETS factors, histone acetylation

44

45

46

47 INTRODUCTION

48 Spatial specific gene expression is fundamental to controlling cell identity in
49 embryonic tissue. Early in the mesenchyme of the developing mammalian limb bud there
50 are no observable morphological differences or histological boundaries; nevertheless, the
51 limb bud is initially polarised along the anterior-posterior axis (Tickle et al 2015) establishing
52 a specialised compartment of cells at the posterior margin called the zone of polarising
53 activity (ZPA). The function of the ZPA is the expression of *Shh*, which operates as a
54 morphogen and a mitogen to coordinate digit formation by integrating growth with digit
55 specification during limb development (Towers et al., 2008; Zhu et al., 2008). A highly
56 conserved ~780 bp enhancer called the ZRS controls the spatiotemporal expression of the
57 *Shh* gene in the ZPA of both the fore and hind limbs (Lettice et al., 2002, 2003; Sagai et al.,
58 2005). The ZRS lies in an intron of the ubiquitously expressed *Lmbr1* gene at a distance of
59 1Mb from the *Shh* gene in human. Well over 20 different point mutations occurring in the
60 ZRS are associated with the misregulation of *Shh* and consequently, to limb skeletal defects.
61 These include preaxial polydactyly type 2 (PPD2), triphalangeal thumb polysyndactyly
62 (TPTPS), syndactyly type IV (SD4), and Werner's mesomelic syndrome (WMS), collectively
63 referred to as ZRS-associated syndromes (Lettice et al., 2003, 2008; Farooq et al., 2010;
64 Furniss et al., 2008; Gurnett et al., 2007; Semerci et al., 2009; Wiczorek et al., 2010).

65 The regulatory mechanisms that direct gene expression to embryonic compartments
66 are not well established in mammalian development; therefore, to understand the events
67 that occur, it is crucial to investigate the activation of spatiotemporal specific enhancers
68 during this process. We previously showed that members of the ETS transcription factor
69 family (Sharrocks, 2001) are involved in the spatial pattern of *Shh* expression (Lettice et al.

2012). Occupancy at multiple ETS sites, which bind the factors GABP α and ETS1, regulates the position of the *Shh* expression boundary in the limb, thus defining the ZPA. In contrast, binding sites for ETV4 and ETV5 in the ZRS, when occupied, repress ectopic *Shh* expression outside the ZPA. A single base pair change is able to subvert this normal developmental process to give rise to skeletal abnormalities. For example, two different human PPD2 point mutations generate additional ETS binding sites, thereby, de-repressing expression of *Shh* in the anterior limb bud. The balance between binding of the activators and repressors is crucial for normal *Shh* expression and the mutations that disrupt this balance result in skeletal defects.

Analysis of developmental gene regulation must also take into account the mechanisms of long-range enhancer/promoter interactions. Previously, we showed that the ZRS contains two domains with distinct activities; one domain, the 5' end of the ZRS (472bp), directs the spatiotemporal activity and the second domain, the 3' half (308bp), is required to mediate activity over long genomic distances (Lettice et al., 2014). Additionally higher-order chromatin conformational changes that occur in the *Shh* locus play a role in gene expression. Elevated frequencies of *Shh*/ZRS co-localisation were observed only in the *Shh* expressing regions of the limb bud (Amano et al., 2009), in a conformation consistent with enhancer-promoter loop formation (Williamson et al., 2016). However, the domain between *Shh*-ZRS is highly compacted in all tissues and developmental stages analysed independent of *Shh* expression.

Here, we investigate the stepwise events that mediate the spatiotemporal activation of an enhancer during development. We demonstrate that even though the activity of the ZRS is restricted to the ZPA, it retains features of a poised enhancer along the full distal portion of the limb bud composed of the mesenchymal cells of the progress zone; whereas,

94 H3K27ac is enriched just in the distal-posterior limb region. We show that FGF signaling
95 plays a key role in priming the ZRS as indicated by an increase in H3K4me1 at the enhancer.
96 In addition, we show the mechanism of acetylation/deacetylation that GABP α , an activator,
97 and ETV4, a repressor, employ to restrict and promote ZRS activation in the distal limb bud.

98

99 **RESULTS**

100 **Modifications of chromatin at the ZRS differ in different regions of the limb bud**

101 In order to characterize specific features of the *Shh* limb enhancer, the ZRS, in
102 different regions of the developing limb, we micro-dissected the limb bud at embryonic day
103 11.5 (E11.5) into several defined segments. Firstly, we examined the distal region which
104 contained the specialised epithelial structure called the AER (apical ectodermal ridge), the
105 mesenchyme of both the progress zone, and the ZPA and in addition, the proximal region
106 which contained the shank of the limb bud (Fig. 1A). Chromatin immunoprecipitation
107 analysed by quantitative PCR (ChIP-qPCR) was performed on the dissected limb tissue for
108 the two modified histones, H3K4me1 and H3K27ac (Fig. 1B). Previous studies demonstrated
109 that these modifications are markers for enhancer activity. H3K4me1 is a predictive
110 chromatin signature for both poised and active enhancers in the human genome,
111 (Heintzman et al.,2007) but in association with H3K27Ac, these mark active regulatory
112 elements (Rada-Iglesias et al., 2012; Cotney et al., 2012). We found specific enrichment of
113 H3K4me1 at the ZRS in the distal region of the dissected E11.5 limb buds, which was
114 appreciably lower in the proximal region of the limb buds. Further dissections of the distal
115 limb bud into anterior and posterior halves enabled us to discern more precisely the
116 location of the H3K4me1 at the ZRS (Fig. 1B). Even though *Shh* was not expressed in the

117 anterior region of the limb bud, the H3K4me1 mark was enriched in both dissected halves
118 suggesting that the ZRS was poised across the distal compartment of the limb.

119 H3K27ac, in contrast, was differentially enriched in the distal mesenchyme greater in
120 the posterior portion of the limb bud. To investigate acetylation of histone H3 across the
121 large 770bp enhancer, two sets of PCR primers were used to amplify each end of the ZRS.
122 The ZRS encompasses two distinct regulatory activities; one residing in the 5' half driving
123 spatiotemporal expression and one residing in the 3' half mediating long range activation of
124 the *Shh* gene (Lettice et al., 2014) (Fig. 1C). Analysis of each half of the enhancer after CHIP
125 identified differential acetylation of H3 across the ZRS. PCR primers complementary to the
126 5' spatiotemporal half (5'ST primers) of the ZRS showed an increase in H3 acetylation
127 compared to the 3' long-range (3'LR primers) end. H3K27ac was associated with the 5' end
128 of the ZRS and was enriched in the distal region of the limb bud. H3K27ac was, therefore,
129 associated with the distal, posterior quadrant of the limb bud consistent with the presence
130 of the ZPA where the *Shh* gene is transcriptionally active (Fig. 1A). Hence, in the case of the
131 ZRS, the enhancer is poised throughout the posterior distal mesenchyme; further events
132 occur to activate the enhancer for productive transcription in the ZPA.

133 We next assessed the chromatin state of the ZRS in the distal region of the limb bud
134 using chromatin immunoprecipitation coupled with microarray called ChIP-on-chip. The
135 chromatin immunoprecipitation analysis using antibodies to H3K4me1 and H3K27ac
136 highlighted the specificity of the histone modifications over the ZRS (Fig. 1D). The pattern of
137 the H3K4me1 covered the extent of the ZRS; whereas, the pattern of H3K27ac, as predicted
138 by the PCR primers, was not centered over the ZRS but was skewed toward the 5' side.
139 Thus, the ZRS exists in differential chromatin states in the limb depending on position and
140 gene activity.

141 **A limb-derived cell line shows ZRS activation and *Shh* induction**

142 To investigate the dynamics of *Shh* regulation in relation to the ZRS, we generated
143 immortalised cell lines from early limb bud mesenchyme (Williamson et al., 2012). RNA-seq
144 analysis of the 14Fp cell line (cells derived from the distal/posterior part of the limb at E
145 11.5) shows that many of the key genes found in the posterior limb bud are expressed with
146 a notable exception being *Shh* (FIG. 2-SUPL. 1A). We performed CHIP-on-chip using
147 antibodies against H3K4me1 and H3K27ac which revealed that, H3K4me1 marked the full
148 extent of the ZRS in the cell line; whereas, H3K27ac was not enriched, demonstrating that
149 the ZRS resides in a poised state reflecting the origin of the cell line from the distal
150 mesenchyme of the limb bud (Fig. 2A and FIG. 2-SUPL. 1A).

151 The poised state of the ZRS in the cells indicated that *Shh* inactivation was due to the
152 lack of specific factors that are responsible for fully activating the ZRS. Previous attempts to
153 activate *Shh* expression in limb bud derived cells using cocktails of known developmental
154 activators such as FGFs and retinoic acid or transfection with HoxD genes have shown that
155 *Shh* is refractory to activation (Kimura et al., 1998). Our attempts with known *Shh* activators
156 confirmed these observations (FIG. 2-SUPL. 2A); however, the drug trichostatin A (TSA), a
157 histone deacetylase (HDAC) inhibitor, stimulated expression (FIG. 2-SUPL. 2B-C). *Shh*
158 expression was detectable within 6h of treatment (FIG. 2B) reaching a maximum at ~24hrs.
159 To further investigate *Shh* activation in the cell line, we carried out a TSA time course to
160 assay H3K27ac enrichment at the ZRS. H3K27ac enrichment was observed over both the ZRS
161 and the *Shh* promoter at 16h of treatment, reaching a maximum at 24h (Fig. 2C),
162 accordingly, with the *Shh* expression time course (Fig. 2B). The fold enrichment of H3K27ac
163 in the limb buds [Fig. 1B] and cell lines [Fig. 2C] seemed dramatically different; therefore,

164 enrichment of H3K27ac was directly compared between the limbs buds and the cells in the
165 same experiment showing that the magnitude of enrichment is comparable [FIG. 2-SUPL.
166 3A].) In the cell lines, the correlation between *Shh* induction of expression and recruitment
167 of H3K27ac suggests that the ZRS is involved in the activation of the transcriptional process.
168 In addition H3K27ac was more highly associated with the region involved in the
169 spatiotemporal activity of the ZRS (as shown using the 5'ST primers). Two control mouse cell
170 lines were used to investigate the specificity of *Shh* activation in the 14Fp cells. Firstly, the
171 mouse ES cell line, E14, which in response to retinoic acid induces *Shh* expression and
172 secondly, an immortalised mesenchymal cell line from the embryonic mandible at E11.5,
173 called the MD cell line were used. In both cell lines, the histone mark, H3K4me1, was not
174 enriched over the ZRS, and TSA treatment did not lead to *Shh* induction after 24h of
175 treatment (FIG. 2-SUPL. 3B-C).

176 Extragenic transcription sites correlate with active regulatory elements and in accord
177 are occupied by RNA Pol II (De Santa et al., 2010, Kim et al., 2010). Genome-wide studies
178 highlighted Pol II occupancy and the synthesis of noncoding transcripts at active enhancer
179 sites, the roles of which, so far, remain unclear. In order to confirm the limb specific
180 enhancer activation, PolII ChIP-qPCR was carried out in limb cells after TSA treatment. In the
181 untreated 14Fp cell line, even though the enhancer is in a poised state, PolII was not
182 appreciably enriched at the *Shh* promoter nor at the ZRS (Fig. 2D). After activation with TSA,
183 PolII was detected at both sites confirming the association of PolII recruitment to the
184 enhancer and the promoter, further suggesting that TSA mediated *Shh* activation in 14Fp
185 involves the ZRS. Thus, this cell line derived from early limb bud mesenchyme showed that
186 the ZRS could be induced to undergo modifications consistent with enhancer activation and

187 concomitantly, *Shh* expression was activated. To further establish the role for ZRS in the
188 activation of *Shh* expression in the cell line, the interaction of the ZRS with its target
189 promoter was analysed.

190 **Promoter-enhancer contacts are established during *Shh* gene activation**

191 *Shh* gene activation is linked to an increase in the level of the H3K27ac histone mark
192 over the ZRS. In order to investigate the reorganization of chromatin structure after TSA
193 treatment and to confirm the involvement of the ZRS in *Shh* activation induced by TSA,
194 circularized chromosome conformation capture (4C-seq) (Stadhouders et al., 2013) analysis
195 was carried out at 18 and 24 hours after TSA treatment (FIG. 2-SUPL. 3D-F). Evidence of
196 increased colocalisation of the ZRS and the *Shh* gene in the expressing region of the limb
197 bud was demonstrated previously by FISH and 3C analysis (Amano et al., 2009, Williamson
198 et al., 2015). 4C-seq analysis in the 14Fp cell line (Fig. 3A) showed marked and highly
199 significant ZRS–*Shh* interactions in the TSA treated cells. The interaction between
200 the *Shh* gene and the ZRS was confirmed by 3C-qPCR (FIG. 3-SUPL. 1E).

201 The fragment containing the promoter site of *Shh* colocalizes with the ZRS and was
202 detected at 18 hours and at 24 hours after TSA treatment (TSA minus : $q < 1.5 \times 10^{-5}$; TSA^{18h} :
203 $q\text{-value} < 5 \times 10^{-10}$; TSA^{+24h} : $q < 7.8 \times 10^{-35}$); whereas, significant contact in the fragment
204 containing the promoter was undetectable in the untreated cells. *Shh*/ZRS proximity in the
205 nucleus occurs regardless of whether the gene or enhancer is active (Williamson et al.,
206 2016); however, in TSA treated cells reorganization in chromatin structure occurs due to
207 activation of the ZRS increasing interactions with the promoter.

208 **FGF signalling is responsible for priming the ZRS**

209 At an early stage of limb development, *Fgf10* expression in the distal limb bud mesenchyme
210 is important for both limb bud outgrowth and induction of FGF signalling from the AER
211 (Ohuchi et al. 1997) which, in turn, maintains the cells of the progress zone. Subsequently,
212 the FGFs function to maintain *Shh* expression in the ZPA (Laufer et al. 1994; Niswander et al.
213 1994; Crossley et al. 1996; Vogel et al. 1996; Ohuchi et al. 1997). We tested the hypothesis
214 that localized FGF expression is correlated with the poised state of the ZRS. Firstly, the 14Fp
215 cell line pre-treated with nintedanib (NIN), a potent broad spectrum inhibitor of FGFR1/2/3,
216 VEGFR1/2/3 and PDGFR α/β (Hillberg et al., 2008) showed a significant reduction in *Shh* after
217 TSA treatment (Fig. 4A). Previous studies shows that an increase in AER-FGF levels leads to
218 gradual repression of *Grem1* in the distal mesenchyme as part of an inhibitory feedback
219 loop (Fgf/Grem1 loop) (Verheyden et al., 2008) and promotes expression of *Etv4* (Mao J et
220 al., 2009). Hence, as control for the efficiency of the FGF inhibition, *Grem1* and *Etv4* levels
221 were evaluated (Fig. 4B) after 4h incubation with NIN or after 4h NIN plus FGF8/10
222 incubation. Since nintedanib can also inhibit VEGF and PDGF receptors, another FGFR
223 inhibitor, BGJ398 (BGJ), was also tested for *Grem1* and *Etv4* expression. Increased levels of
224 *Grem1* were observed after 4h of NIN and BGJ incubations while *Etv4* levels were reduced.
225 The FGF8/10 treatment was sufficient to restore the original levels of both *Grem1* and *Etv4*.
226 To investigate the action of FGF signalling at the ZRS, ChIP for H3K4me1 in the limb specific
227 cell line exposed to NIN was performed (Fig. 4C). As control, a region of the first intron of
228 *Rbm33*, a neighbouring gene, which displays open chromatin coincident with a peak of
229 H3K4me1 was examined. The H3K4me1 enrichment over the ZRS was dramatically reduced
230 after inhibition of FGF activity and TSA treatment did not rescue the presence of this histone
231 modification; whereas, *Rbm33* intron 1 was not significantly affected. The same effect was
232 caused by BGJ on H3K4me1 enrichment (FIG. 4-SUPL. 1D-E), and no differences were

233 observed in comparison with NIN treatment. To assess whether the NIN or BGJ treatment
234 would affect cell survival or cause other abnormality trypan blue staining was performed
235 and no alterations were observed after 4h treatment (FIG. 4-SUPL. 1A).

236 To determine if FGF plays a similar role in effecting the poised state of the ZRS in the
237 embryo, we developed a short-term organ culture approach (Havis E. et al. 2014). Distal tips
238 of E11.5 limb buds were dissected, maintained in media and exposed to NIN for 4h to
239 examine the state of endogenous ZRS. In agreement with the cell line results, the distal tips
240 lost ZRS enrichment of H3K4me1 and higher levels of *Grem1* expression were observed (Fig.
241 4F-G). On the other hand, when proximal dissections of E11.5 limb bud, where the enhancer
242 is in an inactive state, are exposed to a combination of FGF8 and FGF10 the ZRS displays the
243 poised state (Fig. 4H, FIG. 4-SUPL. 1F) showing enrichment of H3K4me1. These data suggest
244 that FGF signalling has a key role in priming and maintaining the ZRS as a poised enhancer in
245 the distal mesenchyme of the limb bud, delineating the boundaries where *Shh* can be
246 potentially expressed. Trypan blue staining was performed on limb dissections by following
247 a reported protocol with slight modifications (Siddique Y.H 2012) (FIG. 4-SUPL. 1B). No signs
248 of increased cell death was observed after 4h of NIN treatment.

249

250 **GABP α activates *Shh* expression**

251 The 14Fp cells retain the expression of some of the ETS genes (FIG. 2-SUPL. 1A)
252 which were shown to play a regulatory role at the ZRS (Lettice et al., 2012). One of these,
253 GABP α , interacts with the ZRS in the limb bud and activates *Shh* expression. In addition
254 others have demonstrated (Kang et al., 2008) that GABP α recruits the co-activator histone
255 acetyltransferase CBP/p300. Therefore, binding of GABP α to the ZRS and recruitment of

256 p300 was examined in the 14Fp cell line (Fig. 5A). CHIP-on-chip analysis on untreated cells
257 for both GABP α and p300, showed an overlapping peak of enrichment for both factors,
258 suggesting a co-occupancy over the ZRS. To further study the interaction between these TFs,
259 we performed co-immunoprecipitation experiments on nuclear extracts from 14Fp cells
260 transfected with GABP α tagged with three copies of the flag epitope. Immunoprecipitation
261 of endogenous p300 co-precipitates the flag-GABP α indicating an association between these
262 two factors (FIG. 5B). Western blot for p300, normalised against the histone H3 showed that
263 p300 levels were not affected (FIG. 5-SUPL. 1B). Based on the assumption that GABP α and
264 p300 together have an important, yet undefined role in the activation of the regulatory
265 element, we next addressed whether the presence of GABP α /p300 influenced ZRS
266 activation. *Shh* expression was examined in cells induced with TSA after reduction of *Gabpa*
267 expression. *Gabpa* siRNA knockdown (Fig. 5C) revealed decreased *Shh* expression after TSA
268 treatment (Fig. 5D). Conversely, overexpression of *Gabpa*, using a doxycycline inducible
269 vector leads to activation of *Shh* (Fig. 5E, FIG. 5-SUPL. 1A). In addition, CHIP analysis for
270 H3K27ac in cells overexpressing GABP α showed an appreciable enrichment over the ZRS;
271 whereas, the transcription factor ETV4, a repressor (see below) which restricts expression
272 outside the ZPA, is displaced from the ZRS (Fig. 5F). Under these conditions, enrichment of
273 GABP α and p300 over the ZRS is also observed (Fig. 5G). These data suggest that GABP α
274 regulates *Shh* expression by modulating the acetylation status of H3K27 of the ZRS.
275 Furthermore, FGF signalling plays a central role, since both GABP α and p300 are released
276 from the ZRS when FGF signalling is inhibited by NIN and the enhancer is no longer poised
277 (Fig. 4D,E). FGF, therefore, mediates priming of the ZRS enabling the binding of GABP α
278 which, in turn, recruits p300.

279 **ETV4 carries out its repressive role via interacting with HDAC2**

280 ETV4/ETV5 binding represses *Shh* expression outside the ZPA in the limb bud (Lettice
281 2012). Since there is a close association between GABP α and p300, we investigated the
282 possibility that the repressive role of ETV4/ETV5 was related to HDAC activity. In order to
283 investigate specific HDAC candidates, RNA-seq data obtained from the cell line and the
284 distal and proximal portions of the limb bud showed nearly all the HDAC classes are
285 represented in both 14Fp and in limb tissue between the cells and the tissue, with the
286 exception of HDAC9 (FIG. 2-SUPL. 1B). Most of the HDACs represented were subjected to
287 CHIP in 14Fp (HDAC1,2,3,4,5,6,8 and 9) and HDAC2 appeared significantly enriched over the
288 ZRS (data not shown) and is one of the most abundant *Hdac* in the RNA samples analysed
289 (FIG. 2-SUPL. 1B). To further examine the role of HDACs in ZRS activity, *Hdac2* and *Hdac1*
290 expression levels were reduced by specific siRNAs in 14Fp cells (Fig. 6A). Both are class I
291 HDACs and often work in concert. *Hdac1* down-regulation had no effect on *Shh* expression,
292 while the reduction of *Hdac2* levels (by siRNA) in 14Fp showed an increase in *Shh* levels.
293 Simultaneous reduction of both *Hdac1* and *Hdac2* did not have an additive effect on the
294 induction of *Shh* (Fig. 6A). To investigate the relationship between the repressor activity of
295 the ETV genes and HDAC2, we performed ChIP-on-chip for these two factors to visualize
296 their distribution over the ZRS (Fig. 6B). Since in the 14Fp cell line ETV5 expression is low
297 (approx. 8-10 fold lower than ETV4) (FIG. 2-SUPL. 1A-B), depletion of ETV5 activity was not
298 necessary in this analysis. ETV4 exhibits two peaks encompassing the ZRS which correspond
299 to the two ETV4 binding sites (Lettice et al., 2012); interestingly, the HDAC2 peak
300 overlapped one of these peaks located at the 3' end which encodes the long range activity
301 of the regulatory element (Lettice et al., 2014). We next tested if HDAC2 and ETV4 were able
302 to physically interact; analysis showed that endogenous ETV4 co-immunoprecipitated with
303 HDAC2 (FIG. 6C). In addition, the negative role of ETV4 on *Shh* expression in 14Fp cells (Fig.

304 6D) was investigated. *Etv4* levels were reduced with siRNA, resulting in a ~40% decrease in
305 *ETV4* and a significant activation of *Shh* expression (Fig. 6D). ChIP using anti-ETV4 and
306 HDAC2 antibodies performed on TSA-treated cells showed that ETV4 together with HDAC2
307 are displaced from the ZRS (Fig. 6E), suggesting that ETV4 opposes GABP α activity by
308 maintaining lower levels of H3K27ac.

309 **DISCUSSION**

310 **The distal limb bud is poised for expression**

311 The ZPA is the organizing center of the early developing limb bud and the restricted
312 expression of *Shh* at this location along the posterior boundary is crucial for correct
313 specification of digit identity and number. Various regulatory inputs are essential to acquire
314 this spatial specific pattern of expression. We showed that an initial input is the event that
315 primes the ZRS, such that the enhancer is poised but transcriptionally inactive. The ZRS
316 priming occurs in a broad region of the distal limb bud mesenchyme that includes tissue that
317 will not express *Shh* in addition to the ZPA. Furthermore, we undertook studies to identify
318 the signalling pathway involved in the induction of ZRS priming. Distal limb mesenchyme,
319 referred to as the progress zone, is known to be under the influence of the FGFs produced in
320 the AER (Laufer et al. 1994; Niswander et al. 1994; Crossley et al. 1996; Vogel et al. 1996;
321 Ohuchi et al. 1997) and we showed that FGFs can induce ZRS priming in distal mesenchyme;
322 whereas, inhibition of FGF signalling results in chromatin changes and loss of H3K4me1 and
323 loss of transcription factor binding suggesting that the ZRS is no longer recognized as a
324 poised enhancer and is in a 'closed' configuration. Thus, one role of FGF signalling is the
325 establishment and maintenance of ZRS priming. Activation of the ZRS, therefore, appears to
326 be a two-step process; ZRS priming occurring broadly in the distal mesenchyme which is a

327 prerequisite for subsequent action by other signals in the posterior region containing the
328 ZPA to activate the ZRS.

329 The poised state of the enhancer is notable in light of the response of the ZRS to the
330 point mutations that cause preaxial polydactyly type 2 and other associated skeletal
331 abnormalities (Anderson 2012). These mutations cause mis-regulation of *Shh* expression in
332 the developing limb bud such that *Shh* expression occurs at an ectopic anterior site in the
333 distal mesenchyme in addition to the ZPA. Ectopic expression of all ZRS mutations
334 examined, thus far, is restricted to the distal mesenchyme suggesting that there is a
335 requirement for the ZRS to be in a poised state in order to be activated and demonstrates a
336 mechanism for *Shh* ectopic activation restricted to the distal mesenchyme of the limb bud.

337 **Levels of GABP α and ETV4 regulate *Shh* expression**

338 Attempts to understand how developmental enhancers operate over such large
339 distances have led to the general idea that chromatin looping assists the interactions of a
340 long-range enhancer with its target promoter (Sanyal et al., 2012). In the limb bud, 3C assay
341 revealed a physical interaction between the ZRS and the promoter (Amano et al., 2009).
342 Here, we confirmed , that upon activation of *Shh* expression in the limb-derived cell line,
343 there is highly specific co-localization of the ZRS with the *Shh* promoter fragment. Thus, the
344 *Shh* limb regulator in the cell line exists in two states; one in which the ZRS is poised
345 reflecting its origin from the distal mesenchyme of the developing limb bud and secondly, in
346 an active state in which the ZRS and the promoter recruit PolII and interact. Hence, the cell
347 line reveals the chromatin dynamics that occur during long-range activation.

348 GABP α /ETS1 and ETV4/ETV5 have antagonistic effects on *Shh* activity in the limb.
349 Occupancy at multiple GABP α /ETS1 sites in the ZRS regulates the position of the ZPA
350 boundary, whereas ETV4/ETV5 binding acts as repressors to restrict expression outside the

351 ZPA. We have hypothesized that the balance between these activator and repressor factors
352 are responsible for regulating activity levels in the developing limb bud (Lettice et al, 2012).
353 Here, we showed that GABP α and ETV4 bind to the ZRS in the cell lines similar to that in the
354 limb bud. GABP α is associated with p300 histone acetyltransferase at the ZRS in the cell
355 lines. Previous reports demonstrated that GABP α , physically interacts with p300 in myeloid
356 cells (Resendes et al., 2006). Activation of AChR (nicotinic acetylcholine receptor) genes in
357 subsynaptic nuclei in adult skeletal muscle is mediated by GABP α , which recruits the histone
358 acetyl transferase (HAT) p300 to the AChR ϵ -subunit promoter (Ravel-Chapuis et al., 2007).
359 Furthermore, the surface of the GABP α OST domain binds to the CH1 and CH3 domains of
360 the co-activator histone acetyltransferase CBP/p300 (Kang H-S, 2008). Here, we showed in
361 the limb-derived cells that a similar interaction of these two factors occurs. In addition,
362 overexpression of GABP α results in an increase in the levels of H3K27ac at the ZRS. A
363 correlation between *Gabpa* expression and the presence of ETV4 at the ZRS is also
364 observed; in that, expression of *Gabpa* results in a displacement of ETV4 at the enhancer.
365 Thus GABP α operates at the ZRS to increase levels of H3K27ac by recruiting p300 and
366 decreasing levels of the repressor ETV4.

367 ETV4 appears to operate in the opposite manner and is one of the dominant factors
368 in maintaining the ZRS in a poised state. Reduction of ETV4 levels is sufficient to activate *Shh*
369 expression. ETV4 interacts with HDAC2 and we further showed the co-localisation of HDAC2
370 and ETV4 at the ZRS in the cell line. Similar to the downregulation of ETV4 the knockdown of
371 HDAC2 induces *Shh*. Activation of *Shh* by TSA releases ETV4 and HDAC2 from the ZRS.
372 Hence activation of the ZRS by both the overexpression of GABP α and treatment with TSA is
373 associated with loss of ETV4 binding which acts directly on histone deacetylase activity.

374 The FGFs play a central role in *Shh* expression by ensuring that the ZRS maintains its
375 primed state throughout the distal limb mesenchyme. This widespread priming, however,
376 opens the ZRS for potential ectopic activation as occurs in preaxial polydactyly and
377 associated phenotypes (Anderson 2012). ETV4 is a repressor that restricts this activity and
378 FGF signalling also induces the levels of ETV4 in the distal mesenchyme of the limb bud
379 (Mao et al., 2009; Zhang et al., 2009). The FGFs, therefore, operate by regulating two
380 contrasting events; firstly, by effecting the chromatin in the distal mesenchyme ensuring
381 that the ZRS is maintained in a poised state and secondly, acting counter to enhancer
382 activation by inducing the level of a repressor that ensures *Shh* expression does not occur
383 outside the region of the ZPA.

384

385 **MATERIALS AND METHODS**

386 **Cell Lines, Transfections, and Treatments.**

387 The 14FP cell line was derived from the posterior third of distal forelimb buds from an
388 Immortomouse (H-2k-tsA58)(Jat et al. 1991). Cells are plated in DMEM (Invitrogen) with
389 10% Foetal Calf Serum (Sigma), Penicillin/Streptomycin and 20 ng/ml Interferon
390 (Peprotech). Cells are grown at 33°C the permissive temperature for the temperature-
391 sensitive T antigen and were passaged as necessary but no later than passage 12. Cells
392 biological replicates are intended as cells cultured separately and treated/analysed at a
393 different passage. Cellular identity was confirmed by RNA expression analysis of specific
394 genes and immortomouse markers and verified to be mycoplasma free. Knock-down of
395 endogenous proteins was performed in 14fp cells after siRNA transfection using Dharmafect
396 1 solution (Dharmacon). Briefly, cells were seeded in 6-well plates to 40% confluence and

397 after 24 hr were transfected using 25 nM of each siRNA pool and 10 μ l of the transfection
398 reagent. The transfection medium was replaced after 12 hr and cells were grown for
399 another 12 hr. Cells were collected 24 hr after the transfection for analyses. siRNA pools
400 were purchased from Thermo Fisher Scientific (Ambion): Gabp α (s66354,s66355),
401 Etv4(s71463, s201776), Hdac2 (s67417, s67416), Hdac1(s119557, s119558) and
402 nontargeting siRNAs (control) (D-001810-02). The siRNA were used separately. Unless
403 otherwise specified, the cells were treated with HDAC inhibitors trichostatin A (TSA; 1 μ M)
404 for 24h before cell harvest and nintedanib (NIN; 100 nM) and BGJ398 (BGJ; 2.5 μ M) for 4h.
405 Cell cultures where incubated, when necessary with 500 ng/ml of FGF10 (R&D Systems, cat.
406 no. 345-FG) and 100 ng/ml of FGF8 (ABCAM, ab205522) combination for 6h after NIN
407 treatments.

408 **Mouse Limb Cultures**

409 Limb buds were dissected from E11.5 mouse embryos and cultured as described by Havis E.
410 et al. (2014) with the following modifications. Limb dissections obtained from different
411 embryos were considered as biological replicates. Briefly distal dissections were treated
412 with nintedanib (NIN.; 100 nM) for 4h. Proximal dissections were incubated with 500 ng/ml
413 of FGF10(R&D Systems, cat. no. 345-FG) and 100 ng/ml of FGF8 (ABCAM, ab205522)
414 combination for 6h. inhibitors were diluted in DMSO. Media with buffers only were used as
415 controls. After treatments, explants were processed for RT-q-PCR or CHIP.

416 Trypan blue staining was performed on limb dissections by following a reported protocol
417 with slight modifications (Siddique Y.H 2012). Total limb dissections were collected and
418 treated 4h with NIN. or media alone. The limbs were then transferred to trypan blue
419 stain and kept in shaking condition for 20 min. 8 limb dissections were directly stained after

420 collection (T0). The samples were washed thoroughly with PBS solution again for 15 more
421 minutes and observed by microscope and imaged to check for any cell damage

422 **Chromatin Immunoprecipitation and antibodies**

423 Crosslinked ChIP was performed as described (Stock et al., 2007) from approximately 10^7
424 cells per experiment. All antibodies used in this study have been previously reported as
425 suitable for ChIP and/or ChIP-seq, p300 (sc-585, Santa Cruz Biotechnology), H3K4me1
426 (ab8895, Abcam), H3K27ac (s39133, Active motif), HDAC2 (ab16032), GABP α (sc-22810,
427 Santa Cruz), with the exception at ETV4 (ABE635, Millipore). All statistical analyses were
428 performed using a two-tailed Student's *t*-test.

429

430 **3C and 4C**

431 3C was conducted according to the protocol described by Stadhouders (2014) et al with
432 minor alterations. In brief cells were treated with 1 mM TSA for 18 and 24 hr or DMSO as a
433 control and fixed in 2 % formaldehyde solution for 10 min. 0.125 M glycine was used to
434 quench the reaction. After a PBS wash and 15 min incubation in lysis buffer, the solution
435 was spun down and nuclei stored at -80 °C until needed. If more than 5×10^5 cells were
436 used, pellets were made up in $1.2 \times$ restriction buffer and divided into 4 aliquotes to reduce
437 formation of aggregates. Primary restriction enzyme digestion was conducted using 800 U
438 Hind III-HF restriction enzyme (NEB) at 37 °C on each aliquot. Before ligation aliquots were
439 combined and T4 DNA ligase (NEB) added and incubated at 16 °C overnight. Hind III digested
440 samples were analysed on a 0.6 % agarose gel and appear as high molecular weight smear
441 running from roughly 4 - 12 kb (FIG. 2-SUPL. 3D- FIG. 3-SUPL. 1A). 3C libraries were analysed

442 on 0.6 % agarose gel and appear as a high molecular weight band (around 12 kb) (FIG. 2-
443 SUPL. 3E- FIG. 3-SUPL. 1B). To this point the 3C libraries were analysed (see below). In order
444 to make 4C libraries a second restriction digest was performed using the 4-cutter MluCI
445 (Roche) at 37 °C overnight and second ligation with T4 DNA ligase (NEB). MluCI digested
446 samples were analysed on a 1.5 % gel appearing as smear between roughly 0.3 - 1kb (FIG. 2-
447 SUPL. 3F). Finally, 4C libraries were purified using QIA quick PCR purification kit (Qiagen) to
448 produce final purified 4C libraries. After PCR amplification and purification (table S2),
449 sequencing adaptors were ligated and 4C libraries sequenced using in-house Ion Proton™
450 sequencing.

451 **Analysis of 4C libraries**

452 De-multiplexed sequencing reads (fastq files) can be summarised: first we trimmed known
453 bait sequence using cutadapt (Martin M 2011) and selected only those reads where known
454 viewpoint-associated sequence was present. Reads were mapped to the mouse reference
455 genome (build mm9) using bowtie2 (Langmead B et al. 2012) with the very-sensitive flag 3.
456 Alignments were filtered with a MAPQ score > 30 to select for high-confidence alignments
457 using samtools (Li H et al. 2009). Contacts were then normalised using the r3cseq R package
458 and assigned FDR q-values to interactions, with the aim of finding those significantly over-
459 represented relative to expectation. The normalisation procedure for 4C data is adapted
460 from a previous method for normalising deepCAGE data between samples (Balwierz PJ et al.
461 2009).

462 **Analysis of 3C libraries**

463 Digestion efficiency and sample purity was assessed as described previously (Hagege H et al.
464 2007). Primers were designed using Primer3 with an anchor primer in the fragment at the 5'
465 end of the ZRS and in potential interacting fragments around the Shh promoter, gene body,
466 3' end and gene desert. Quantitative PCR was carried out using the Roche LightCycler 480
467 SYBR Green I Master and Roche LightCycler 480 probe Master on a Roche LC480 according
468 to the instructions of the manufacturer (Roche). Two PACs, RCPI21-542n10 (148kb long
469 covering Rnf32 to 5' of LMBR1) and RCPI21-508F15 (203kb long covering Shh and 150kb 5')
470 obtained from RPCI21 library (HGMP Resource Centre, Cambridge, U.K.) were used as as a
471 PCR control template. The PAC clones were cut with *HindIII* and equimolar amounts re-
472 ligated by T4 DNA ligase. All primer pairs were tested on a standard curve of the BAC control
473 library and yielded PCR efficiencies >1.7. The presence of a single PCR product was
474 confirmed and melting curves analysed. Cycling conditions were: 95 °C for 5 min, 40 cycles
475 of 95 °C for 15 s, 60 °C for 30 s, 72 °C for 30 s for the. Quantitative PCR data were
476 normalized to ZRS 3'LR ChIP oligos as a loading control. 3C oligos from Splinter E et al (2006)
477 were used to control for interaction frequencies between samples. ZRS 3'LR ChIP
478 oligos cycling conditions were 95 °C for 5 min, 40 cycles of 95 °C for 10 s, 60 °C for 30 s, 72 °C
479 for 30 s. The cycling conditions for the interacting fragments and the anchor were 95 °C for
480 5 min, 45 cycles of 95 °C for 15 s, 60 °C for 1', 72 °C for 1 s. Data analysis was carried out
481 according to Hagege (2007) and is presented as relative crosslinking frequency. The primers
482 used for the chromatin conformation capture interaction studies are listed in table S2.

483 **Chromatin Immunoprecipitation and Tiling Microarrays**

484 Cells from dissected E11.5 limbs and 14fp were fixed with 1% formaldehyde (25°C, 10 min)
485 and stopped with 0.125 M glycine. Crosslinked ChIP was performed as described (Stock et

486 al., 2007). In brief, the nuclei were sonicated using a Diagenode Bioruptor (Leige, full power
487 30s on, 30s off, in an ice bath for 50 min) to produce fragments of <300 bp. Chromatin (350
488 mg) was incubated with 5 mg prebound (to Protein A or G magnetic beads, Invitrogen) IgG
489 (Santa Cruz, sc-2025) or the previously mentioned antibodies, raised to in the presence of
490 50 mg of BSA, washed, and eluted. Reverse crosslinked DNA was purified with Proteinase K
491 (Glenaxxon) and QIAGEN PCR purification kit. qPCR of the CHIP experiments were carried
492 out using equal concentrations of input, IgG and Chip DNA using a Sybr Green (Roche)
493 reaction. From each biological replicate three technical replicates were analysed.
494 Enrichment values for CHIP samples from limb bud sections extracts are presented either as
495 percentage of input or as fold differences relative to IgG and normalized to input with the
496 formula $2^{[(CtIgG-CtInput)-(CtAb-CtInput)]}$ where Ct values are threshold cycles. All biological
497 replicates were carried out in duplicate unless stated. Primers used for ZRS and the controls
498 are shown in the table TS1. For the custom Nimblegen tiling arrays CHIP DNA and input DNA
499 CHIP DNA and input DNA were amplified (WGA2 kit, Sigma), labelled, and hybridized
500 according to the manufacturer's protocol to a 354,999 unique probe custom microarray
501 containing specific tiled regions of the mouse genome (Nimblegen). For the Agilent arrays a
502 custom tiling array was designed including some of the genes involved in limb development,
503 including gene deserts associated with such genes. GEO accession number for the CHIP data
504 is GSE104074.

505 **Nimblegen Arrays**

506 Microarray data were analyzed in R/Bioconductor
507 (<http://genomebiology.com/2004/5/10/R80>) with the Epigenome (PROT43) protocol
508 (<http://www.epigenome-noe.net/WWW/researchtools/protocol.php?protid=43>) with the

509 following parameters. The mean signal intensity of the two replicate probes on each array
510 was taken. Loess normalization was used within arrays to correct for the dye bias, and scale
511 normalization was used within the replicates group to control interarray variability using the
512 R package (Limma et al., 2015). The \log_2 enrichment for each CHIP group was calculated by
513 subtracting the mean of \log_2 input intensities from the mean of d enriched intensities and
514 averaging over the two biological replicates.

515 **Agilent Arrays**

516 The Median Signal was extracted from the scanned image files and processed using the R
517 package (Ringo et al., 2007). Probe intensities were transformed from raw values into
518 background-corrected normalised log ratios (CHIP/Input) using Ringo's preprocess method
519 (VSN normalisation). Smoothing over individual probe intensities was performed using a
520 sliding window of 1000 bp along the chromosome and replacing the intensity at the
521 genomic position by the median over the intensities of those reporters inside the window.

522 **Immunoprecipitation of FLAG Fusion Proteins**

523 The pSV40-Tet3G- pTRE3G-mCherry- Gabp α plasmid was generated using the In-Fusion[®]
524 cloning technology (Clontech, catalogue No 639649). First, the pTRE3G-mCherry vector
525 (Clontech, catalogue Nos 631160 & 631175) was linearized using a unique restriction
526 site between the origin of replication and the Tet-responsive promoter (pTRE3G). Second,
527 the sequences encoding for SV40 promoter, Kanamycin/Neomycin resistance, internal
528 ribosome entry site IRES2 and Tet-ON 3G transactivator were inserted. Third, we removed
529 the Ampicillin resistance cassette. Lastly, the sequence of the self-cleaving peptide P2A was
530 cloned between the mCherry fluorescent marker and the 3xFLAG tagged Gabp α gene, in

531 order to generate a bicistronic expression under the control of the TRE3G promoter and an
532 empty control vector was also used. Overexpression analyses were performed in 14fp cells
533 by transfecting plasmids using Lipofectamine LTX with plus reagent (ThermoFisher) and
534 following standard manufacturer's protocol. Nuclear extracts used in the
535 immunoprecipitation were prepared from 14fp using a NE-PER nuclear and cytoplasmic
536 extraction kit (Thermo Scientific). The nuclear extract was incubated with anti-FLAG M2
537 affinity gel (Sigma) for 3h at 4°C. The beads were washed three times with washing buffer.
538 The immunoprecipitates were eluted with 1× SDS buffer, separated on a 4%–20% Novex
539 Tris-Glycine SDS-PAGE gel (Invitrogen), transferred to a PVDF membrane (Millipore),
540 incubated with anti-FLAG (Sigma) or with anti-GABPα (Santa Cruz, sc-22810).

541

542 **Gene expression analysis, RNA library Preparation, Sequencing and Analysis**

543 Total RNA was prepared using Trizol reagent (Invitrogen) according to manufacturer's
544 protocol (for limb buds, dissected anterior, posterior distal and proximal tissue was
545 dissociated into single cell suspensions in Trizol using a syringe fitted with a 25G (0.5
546 mm) needle (BD Microlance), followed by acid phenol:chloroform:isopropyl alcohol
547 extraction and then digested with 2U DNaseI (Ambion) for 30 minutes at 37°. RNA was
548 reverse-transcribed to cDNA using QuantiTect Reverse Transcription Kit (QIAGEN). The
549 quantitative real-time PCR reactions were performed in a 7300 system (Applied Biosystems,
550 Life Technologies) by using LightCycler® 480 SYBR Green I Master (Roche) and gene specific
551 primer sets for *shh*, *Gabpα*, *Etv4*. The cycle threshold (CT) values from all quantitative real-
552 time PCR experiments were analysed using $\Delta\Delta CT$ method. Data were normalized to
553 glyceraldehyde 3-phosphate dehydrogenase (GAPDH) and expressed as fold changes over

554 that in control treatment group. From each biological replicate three technical replicates
555 were analysed. All statistical analyses were performed using a two-tailed Student's *t*-test.

556 RNA sequencing was conducted by GATC Biotech. Samples were only submitted with an OD
557 260/280 ratio ≥ 1.8 , a 260/230 ratio ≥ 1.7 and a RNA Integrity Number (RIN) value ≥ 8 as
558 detected by Agilent Technologies 2100 Bionalyser. The InViewTM Transcriptome Explore
559 service provided by GATC was used to provide a randomly primed and amplified cDNA
560 library with Illumina adaptors ready for sequencing. Illumina sequencing was conducted
561 producing 50 bp single end reads and a guarantee of over 30 million reads per sample. All
562 samples were analysed on the main Galaxy server by first checking sequence quality by
563 FastQC. Reads were then trimmed and any Illumina sequencing adaptors removed as
564 appropriate and aligned to the mouse genome (mm9, NCBI 37) using Tophat2 (Galaxy Tool
565 Version 0.9). The results for each condition were fed into Cuffdiff (Galaxy Tool Version
566 2.2.1.3) and visualised using the R Bioconductor package CummeRbund (Release 3.2). This
567 process was repeated using RNA isolated from both immortalized limb cell lines and isolated
568 limb tissue. Two biological replicates were analysed for each condition.

569

570 **Acknowledgments**

571 We thank the staff at the Evans Building and especially Anna Thornburn for expert
572 technical assistance. We also thank Prof. N. Hastie and Prof. W. Bickmore for critically
573 reading the manuscript. This work was supported by an MRC core grant. We also thank Dr.
574 Laura Lettice who kindly provided us the PAC vectors and the 3C libraries from anterior and
575 posterior limb tissue.

576

577

578

579 **References**

580 • Amano T, Sagai T, Tanabe H, Mizushina Y, Nakazawa H, Shiroishi T. (2009)

581 Chromosomal dynamics at the Shh locus: limb bud-specific differential regulation of

582 competence and active transcription. *Dev Cell*. 16:47-57.

583 • Anderson E, Devenney PS, Hill RE, Lettice LA. (2014) Mapping the Shh long-range

584 regulatory domain. *Development*. 141:3934-43.

585 • Anderson E, Peluso S, Lettice LA, Hill RE. (2012) Human limb abnormalities caused by

586 disruption of hedgehog signaling. *Trends Genet*. 28:364-73.

587 • Balwierz PJ, Carninci P, Daub CO, Kawai J, Hayashizaki Y, Van Belle W, Beisel C, van

588 Nimwegen E (2009) Methods for analyzing deep sequencing expression data: constructing

589 the human and mouse promoterome with deepCAGE data. *Genome biology*, 10(7): R79.

590 • Cotney J, Leng J, Oh S, DeMare LE, Reilly SK, Gerstein MB, Noonan JP. (2012) Chromatin

591 state signatures associated with tissue-specific gene expression and enhancer

592 activity in the embryonic limb. *Genome Res*. 22:1069-80.

593 • Crossley PH, Minowada G, MacArthur CA, Martin GR. (1996) Roles for FGF8 in the

594 induction, initiation, and maintenance of chick limb development. *Cell*. 12;84:127-36.

595 • De Santa F, Barozzi I, Mietton F, Ghisletti S, Polletti S, Tusi BK, Muller H, Ragoussis J,

596 Wei CL, Natoli G. (2010) A large fraction of extragenic RNA pol II transcription sites

597 overlap enhancers. *PLoS Biol*. May 11;8:e1000384.

598 • Farooq M, Troelsen JT, Boyd M, Eiberg H, Hansen L, Hussain MS, Rehman Su, Azhar

599 A, Ali A, Bakhtiar SM, Tommerup N, Baig SM, Kjaer KW. (2010) Preaxial

600 polydactyly/triphalangeal thumb is associated with changed transcription factor-

- 601 binding affinity in a family with a novel point mutation in the long-range cis-
602 regulatory element ZRS. *Eur J Hum Genet.* 18:733-6.
- 603 • Furniss D, Lettice LA, Taylor IB, Critchley PS, Giele H, Hill RE, Wilkie AO. (2008) A
604 variant in the sonic hedgehog regulatory sequence (ZRS) is associated with
605 triphalangeal thumb and deregulates expression in the developing limb. *Hum Mol*
606 *Genet.* 17:2417-23.
 - 607 • Gurnett CA, Bowcock AM, Dietz FR, Morcuende JA, Murray JC, Dobbs MB. (2007)
608 Two novel point mutations in the long-range SHH enhancer in three families with
609 triphalangeal thumb and preaxial polydactyly. *Am J Med Genet A.* 143A:27-32.
 - 610 • Havis E, Bonnin MA, Olivera-Martinez I, Nazaret N, Ruggiu M, Weibel J, Durand C,
611 Guerquin MJ, Bonod-Bidaud C, Ruggiero F, Schweitzer R, Duprez D. (2014)
612 Transcriptomic analysis of mouse limb tendon cells during development.
613 *Development.* 141(19):3683-96.
 - 614 • Heintzman N, Stuart R, Hon G, Fu Y, Ching C, et al. (2007). Distinct and predictive
615 chromatin signatures of transcriptional promoters and enhancers in the human
616 genome. *Nat. Genet.* 39:311–18
 - 617 • Hilberg F, Roth GJ, Krssak M, Kautschitsch S, Sommergruber W, Tontsch-Grunt U,
618 Garin-Chesa P, Bader G, Zoephel A, Quant J, Heckel A, Rettig WJ. (2008) BIBF 1120:
619 triple angiokinase inhibitor with sustained receptor blockade and good antitumor
620 efficacy. *Cancer Res.* 68:4774-82.
 - 621 • Kang HS, Nelson ML, Mackereth CD, Schärpf M, Graves BJ, McIntosh LP. (2008)
622 Identification and structural characterization of a CBP/p300-binding domain from
623 the ETS family transcription factor GABP alpha. *J Mol Biol.* 377:636-46.

- 624 • Kim TK, Hemberg M, Gray JM, Costa AM, Bear DM, Wu J, Harmin DA, Laptewicz M,
625 Barbara-Haley K, Kuersten S, Markenscoff-Papadimitriou E, Kuhl D, Bito H, Worley
626 PF, Kreiman G, Greenberg ME. (2010) Widespread transcription at neuronal activity-
627 regulated enhancers. *Nature*. 465:182-7.
- 628 • Kimura J, Ide H. (1998) Shh, Bmp-2 and Hoxd-13 gene expression in chick limb bud
629 cells in culture. *Dev Growth Differ*. 40(4):457-64.
- 630 • Langmead B, Salzberg SL (2012) Fast gapped-read alignment with Bowtie 2. *Nature*
631 *methods*, 9(4): 357–9.
- 632 • Laufer E, Nelson CE, Johnson RL, Morgan BA, Tabin C. (1994) Sonic hedgehog and
633 Fgf-4 act through a signaling cascade and feedback loop to integrate growth and
634 patterning of the developing limb bud. *Cell*. 79:993-1003.
- 635 • Lettice LA, Heaney SJ, Purdie LA, Li L, de Beer P, Oostra BA, Goode D, Elgar G, Hill RE,
636 de Graaff E. (2003) A long-range Shh enhancer regulates expression in the
637 developing limb and fin and is associated with preaxial polydactyly. *Hum Mol Genet*.
638 12:1725-35.
- 639 • Lettice LA, Horikoshi T, Heaney SJ, van Baren MJ, van der Linde HC, Breedveld GJ,
640 Joosse M, Akarsu N, Oostra BA, Endo N, Shibata M, Suzuki M, Takahashi E, Shinka T,
641 Nakahori Y, Ayusawa D, Nakabayashi K, Scherer SW, Heutink P, Hill RE, Noji S.
642 Disruption of a long-range cis-acting regulator for Shh causes preaxial polydactyly.
643 *Proc Natl Acad Sci U S A*. 2002 May 28;99(11):7548-53.
- 644 • Lettice LA, Williamson I, Devenney PS, Kilanowski F, Dorin J, Hill RE. (2014)
645 Development of five digits is controlled by a bipartite long-range cis-regulator.
646 *Development*. 141:1715-25.

- 647 • Lettice LA, Williamson I, Wiltshire JH, Peluso S, Devenney PS, Hill AE, Essafi A,
648 Hagman J, Mort R, Grimes G, DeAngelis CL, Hill RE (2012). Opposing functions of the
649 ETS factor family define Shh spatial expression in limb buds and underlie polydactyly.
650 *Dev Cell.* 22:459-67.
- 651 • Li H, Handsaker B, Wysoker A, Fennell T, Ruan J, Homer N, Marth G, Abecasis G,
652 Durbin R (2009) The Sequence Alignment/Map format and SAMtools. *Bioinformatics*,
653 25(16): 2078–2079.
- 654 • Limma Ritchie, M.E., Phipson, B., Wu, D., Hu, Y., Law, C.W., Shi, W., and Smyth, G.K.
655 (2015). limma powers differential expression analyses for RNA-sequencing and
656 microarray studies. *Nucleic Acids Research* 43(7), e47.
- 657 • Mao J, McGlenn E, Huang P, Tabin CJ, McMahon AP. (2009) Fgf-dependent Etv4/5
658 activity is required for posterior restriction of Sonic Hedgehog and promoting
659 outgrowth of the vertebrate limb. *Dev Cell.* 16:600-6.
- 660 • Martin M (2011) Cutadapt removes adapter sequences from high-throughput
661 sequencing reads. *EMBnet.journal*, 17(1): 10–12.
- 662 • Niswander L, Jeffrey S, Martin GR, Tickle C. (1994) A positive feedback loop
663 coordinates growth and patterning in the vertebrate limb. *Nature.* 371:609-12.
- 664 • Ohuchi H, Nakagawa T, Yamamoto A, Araga A, Ohata T, Ishimaru Y, Yoshioka H,
665 Kuwana T, Nohno T, Yamasaki M, Itoh N, Noji S. (1997) The mesenchymal factor,
666 FGF10, initiates and maintains the outgrowth of the chick limb bud through
667 interaction with FGF8, an apical ectodermal factor. *Development.* 124:2235-44.
- 668 • Rada-Iglesias A, Bajpai R, Prescott S, Brugmann SA, Swigut T, Wysocka J. (2012)
669 Epigenomic annotation of enhancers predicts transcriptional regulators of human
670 neural crest. *Cell Stem Cell.* 11:633-48.

- 671 • Ravel-Chapuis A, Vandromme M, Thomas JL, Schaeffer L. (2007) Postsynaptic
672 chromatin is under neural control at the neuromuscular junction. *EMBO J.* 26:1117-
673 28.
- 674 • Resendes KK, Rosmarin AG. (2006) GA-binding protein and p300 are essential
675 components of a retinoic acid-induced enhanceosome in myeloid cells. *Mol Cell Biol*
676 26:3060-70.
- 677 • Ringo Joern Toedling, Oleg Sklyar, Tammo Krueger, Jenny J. Fischer, Silke Sperling,
678 and Wolfgang Huber (2007) Ringo - an R/Bioconductor package for analyzing ChIP-
679 chip readouts. *BMC Bioinformatics*, 8:221.
- 680 • Ristevski S, O'Leary DA, Thornell AP, Owen MJ, Kola I, Hertzog PJ. (2004) The ETS
681 transcription factor GABPalpha is essential for early embryogenesis. *Mol Cell Biol.*
682 24:5844-9.
- 683 • Ristevski S, Tam PP, Hertzog PJ, Kola I. (2002) Ets2 is expressed during
684 morphogenesis of the somite and limb in the mouse embryo. *Mech Dev.* 116:165-8.
- 685 • Sagai T, Hosoya M, Mizushina Y, Tamura M, Shiroishi T. (2005) Elimination of a long-
686 range cis-regulatory module causes complete loss of limb-specific Shh expression
687 and truncation of the mouse limb. *Development.* 132:797-803.
- 688 • Sanyal A, Lajoie BR, Jain G, Dekker J. (2012) The long-range interaction landscape of
689 gene promoters. *Nature.* 489:109-13.
- 690 • Semerci CN, Demirkan F, Ozdemir M, Biskin E, Akin B, Bagci H, Akarsu NA. (2009)
691 Homozygous feature of isolated triphalangeal thumb-preaxial polydactyly linked to
692 7q36: no phenotypic difference between homozygotes and heterozygotes. *Clin*
693 *Genet.* 76:85-90.

- 694 • Sharrocks AD. (2001) The ETS-domain transcription factor family. *Nat Rev Mol Cell*
695 *Biol.* 2:827-37.
- 696 • Siddique Y.H. Protective role of curcumin against the toxic effects of
697 cyclophosphamide in the third instar larvae of transgenic *Drosophila*
698 *melanogaster* (hsp70-lacZ) Bg9. (2012). *Altern. Med. Stud.*, 2 p. 2
- 699 • Splinter E, Heath H, Kooren J, Palstra RJ, Klous P, Grosveld F, Galjart N, de Laat W.
700 CTCF mediates long-range chromatin looping and local histone modification in the
701 beta-globin locus. (2006) *Genes Dev.*; 20(17):2349-54.
- 702 • Stadhouders R, Kolovos P, Brouwer R, Zuin J, van den Heuvel A, Kockx C, Palstra RJ,
703 Wendt KS, Grosveld F, van Ijcken W, Soler E. (2013) Multiplexed chromosome
704 conformation capture sequencing for rapid genome-scale high-resolution detection
705 of long-range chromatin interactions. *Nat Protoc.* 8:509-24.
- 706 • Stock JK, Giadrossi S, Casanova M, Brookes E, Vidal M, Koseki H, Brockdorff N, Fisher
707 AG, Pombo A. (2007) Ring1-mediated ubiquitination of H2A restrains poised RNA
708 polymerase II at bivalent genes in mouse ES cells. *Nat Cell Biol.* 9:1428-35.
- 709 • Tickle C. (2015) How the embryo makes a limb: determination, polarity and identity.
710 *J Anat.* 227:418-30.
- 711 • Towers M, Mahood R, Yin Y, Tickle C. (2008) Integration of growth and specification
712 in chick wing digit-patterning. *Nature.* 452:882-6.
- 713 • Verheyden JM, Sun X. (2008) An Fgf/Gremlin inhibitory feedback loop triggers
714 termination of limb bud outgrowth. *Nature.* 454:638-41.
- 715 • Vogel A, Rodriguez C, Izpisua-Belmonte JC. (1996) Involvement of FGF-8 in initiation,
716 outgrowth and patterning of the vertebrate limb. *Development.* 122:1737-50.

- 717 • Wieczorek D, Pawlik B, Li Y, Akarsu NA, Caliebe A, May KJ, Schweiger B, Vargas FR,
718 Balci S, Gillessen-Kaesbach G, Wollnik B. (2010) A specific mutation in the distant
719 sonic hedgehog (SHH) cis-regulator (ZRS) causes Werner mesomelic syndrome
720 (WMS) while complete ZRS duplications underlie Haas type polysyndactyly and
721 preaxial polydactyly (PPD) with or without triphalangeal thumb. *Hum Mutat.* 31:81-
722 9.
- 723 • Williamson I, Eskeland R, Lettice LA, Hill AE, Boyle S, Grimes GR, Hill RE, Bickmore
724 WA. (2012) Anterior-posterior differences in HoxD chromatin topology in limb
725 development. *Development.* 139:3157-67.
- 726 • Williamson I, Lettice LA, Hill RE, Bickmore WA. (2016) Shh and ZRS enhancer
727 colocalisation is specific to the zone of polarising activity. *Development.* 143:2994-
728 3001.
- 729 • Zakany J, Zacchetti G, Duboule D. (2007) Interactions between HOXD and Gli3 genes
730 control the limb apical ectodermal ridge via Fgf10. *Dev Biol.* 306:883-93.
- 731 • Zhang Z, Verheyden JM, Hassell JA, Sun X. (2009) FGF-regulated Etv genes are
732 essential for repressing Shh expression in mouse limb buds. *Dev Cell.* 16:607-13.
- 733 • Zhu J, Nakamura E, Nguyen MT, Bao X, Akiyama H, Mackem S. (2008) Uncoupling
734 Sonic hedgehog control of pattern and expansion of the developing limb bud. *Dev*
735 *Cell.* 14:624-32.

736

737

738

739 **Figure legends**

740 **Figure 1. H3K4me1 and H3K27Ac distribution over the ZRS in E11.5 limb buds**

741 (A) Representation of an E11.5 mouse limb bud. The AER (orange), the ZPA (yellow) and
742 FGF10 (cyan) are responsible for the anterior/posterior limb patterning and for directing the
743 proliferation of the distal portion of the limb. The limb buds were dissected into anterior-
744 posterior or distal-proximal regions. (B) Chromatin from E11.5 dissected limb buds tissue
745 was enriched by chromatin immunoprecipitation (ChIP) for H3K4me1 and H3K27ac histone
746 modifications. DNA was quantified by qRT-PCR. Means of fold enrichment over nonspecific
747 IgG recoveries and \pm SEM from two independent experiments are plotted. (C) Schematic of
748 the ZRS (dark blue box) lying in intron 5 of *Lmbr1* (blue box), 800kb away from *Shh* gene.
749 Within the ZRS (dark blue box) five ETS binding sites (light blue) and two ETV binding sites
750 (orange) are highlighted. The primers used to evaluate the ChIP experiments are localised
751 over the long-range activity and the spatio-temporal activity sequences, both indicated with
752 a blue line (complete list of oligos in Supplementary file 1). (D) ChIP-on-chip analysis of distal
753 mesenchyme from two biological replicates E11.5 limb buds using antibodies to two
754 different histone modifications (H3K4me1 and H3K27ac). Data for two different genomic
755 regions, the fifth intron of *Lmbr1* gene and the *Shh* gene are shown The y axis is the Log_2 for
756 each ChIP/input DNA and the x axis represents a segment of DNA. The DNA region
757 containing the ZRS is highlighted by the grey shading. As controls, the whole of the *Shh*
758 coding region plus promoter (*Shh*) is shown.

759 **Figure 2. TSA treatment activates *Shh* in a limb derived cell line (14Fp)**

760 (A) ChIP from two biological replicates of E11.5 limb derived cell line (14Fp cell line) using
761 antibodies to two different histone modifications (H3K4me1 and H3K27Ac) analysed by
762 hybridizing to tiling microarrays. Summary is presented using two different genomic regions,

763 the y axis is \log_2 for each ChIP/input DNA and the x axis represents a segment of DNA from
764 the microarray. The DNA region containing the ZRS is highlighted by the grey shading. As
765 controls, the whole of the *Shh* coding region plus promoter is shown. (B) Time course of the
766 expression of *Shh* in E11.5 limb derived cell line after TSA treatment detected by
767 quantitative RT-PCR. The *Shh* levels were evaluated relative to control and normalized to
768 GAPDH expression levels. Data points represent the average of triplicate determinations \pm
769 SEM. (C) Chromatin from 14Fp was harvested 3, 6, 18 and 24 h after TSA treatment or 24h
770 with DMSO as control (ctr). Shown are results from ChIP analysis using anti-H3K27ac
771 antibody. Enrichment of H3K27ac at the 5'ST (grey), 3'LR (blue) and promoter (black) was
772 detected by qPCR and represented as mean of fold enrichment/background (IgG) \pm SEM
773 over three biological replicates; a negative control region was analysed and did not give an
774 appreciable signal (data not shown). (D) Shown are results from ChIP analysis using anti-RNA
775 Pol II antibody after 24h of TSA treatment. Indicated are the *shh* promoter (black), the 5'ST
776 (grey) and control region (yellow). Recovered DNA sequences were quantified as percentage
777 of input and \pm SEM from two independent experiments and are plotted. The IgG did give
778 no detectable signal.

779 **Figure 3. TSA treatment induces a ZRS–SHH interaction.**

780 (A) The profile of 4C-Seq at the ZRS locus in 14Fp cells. Control and TSA treatment after 18h
781 and 24h are shown. ZRS shown as the enhancer (anchor) bait fragment along an
782 approximately 2Mb region of chromosome 5 (UCSC genome browser view of
783 chr5:28,000,000–30,000,000 (mm9). The x axis represents the position on chromosome 5
784 and the y axis the normalised reads as read per million sequences (RPMs). Only highly
785 significant interactions are shown (FDR q-value $< 5 \times 10^{-5}$). The blue bar represents the

786 location of the ZRS (bait) and the red bar represents the *Shh* gene. Each rectangle is a
787 restriction fragment, the dots coloured at the top of each rectangle reflect the FDR q-value
788 indicating the significance of the interaction (legend between A and B). (B) Focus on the *Shh*
789 region (red bar in the zoomed-in view) shows the number of interactions of the bait region
790 with SHH in both untreated and TSA treated (after 24h) samples.

791 **Figure 4. FGFs are crucial in priming *Shh* limb specific enhancer.**

792 (A) qRT-PCR was used to detect the expression levels of *Shh* in 14Fp cell line after TSA and
793 nintedanib (NIN) treatment. The *Shh* levels were evaluated relative to control and
794 normalized to GAPDH levels. Data points represent the mean of three biological replicates
795 +/- SEM. (B) qRT-PCR to detect the expression of *Grem1* (grey bars) and *Etv4* (black bars)
796 after 4 h of nintedanib (NIN), with or without supplement of FGF8/10 for 6 h. Also shown is
797 BGJ treatment. Data points represent the average of duplicate determinations +/- SEM. (C)
798 Chromatin from the 14Fp cell line was harvest after TSA and NIN treatment and CHIP for
799 H3K4me1 was carried out. DNA was quantified by qRT-PCR using the ZRS 3'LR and *Rbm33*
800 oligos. Data are represented as mean \pm SEM of the fold enrichment over nonspecific IgG
801 recoveries from two independent experiments. (D, E) CHIP analyses after NIN treatment
802 where performed to further analyse the enrichment of the transcription factor GABP α and
803 P300 over the ZRS (black) and on a specific genomic control region, *Rbm33* intron (grey).
804 DNA was quantified by qRT-PCR. Mean (\pm SEM) of the fold enrichment over nonspecific IgG
805 recoveries from two independent experiments are plotted. (F) qRT-PCR to detect the
806 expression of *Grem1* in the distal limb bud after 4h of NIN treatment. (G) CHIP of distal and
807 proximal limb tissue from limb buds using an antibody against H3K4me1. Distal limb tissue
808 was treated for 4h with or without NIN. Proximal limb tissue was used as negative control.

809 DNA was quantified by qRT-PCR and fold enrichment over nonspecific IgG recoveries using
810 the ZRS 3'LR oligos and \pm SEM from two independent experiments were plotted. (H)
811 H3K4me1 CHIP of the proximal limb tissue at E11.5 after 4h of exposure to FGF8 and FGF10.
812 Fold enrichment over nonspecific IgG recoveries and \pm SEM from two independent
813 experiments are plotted. DNA was quantified by qRT-PCR using the ZRS 3'LR oligos.

814 **Figure 5. GABP α co-localises with P300 and modulates ZRS acetylation status.**

815 A) Chromatin immunoprecipitation (ChIP) analysis from two biological replicates on the
816 14Fp cell line using GABP α and p300 antibodies using tiling microarrays. Summary is
817 presented using two different genomic regions, the y axis is Log₂ for each ChIP/input DNA
818 and the x axis represents a segment of DNA from the microarray. The DNA region containing
819 the ZRS is highlighted by the grey shading. As controls, the whole of the *Shh* coding region
820 plus promoter is shown. (B) 14Fp nuclear cell extracts from cells stably transfected with
821 3Xflag-Gabp α (FIG. 5-SUPL. 1E) treated with or without doxycycline were analysed by
822 immuno-precipitation with anti-p300 antibody followed by Western blot analysis with anti
823 flag-tag antibody. As control the empty vector plus doxycycline was used. (C) Western blot
824 analysis with anti-GABP α of 14Fp nuclear cell extracts transiently transfected with Gabp α
825 siRNA (siGabp- α) or nonspecific siRNA (siCTR) and TSA treated. (D) Quantitative RT-PCR was
826 used to detect the mRNA levels of *Shh* (grey box) and *Gabp α* (black box) in 14Fp cells
827 transfected with *Gabp α* siRNA or nonspecific siRNA. 18 hours after transfection, the cells
828 were treated with 1 μ M TSA for 24 hours. *Shh* and *Gabp α* levels were evaluated relative to
829 control and normalized to GAPDH levels from two biological replicates. (E) Quantitative RT-
830 PCR to detect the mRNA levels of *Shh* (black box) and *Gabp α* (grey box) in 14Fp cells stably
831 transfected with 3Xflag-Gabp α vector and an empty vector as control. Data points represent

832 the mean \pm SEM of three biological replicate. (F) Chromatin from 14Fp cells stably
833 transfected with 3Xflag-*Gabpa* vector and an empty vector as control was analysed by ChIP
834 for H3K27Ac histone modification and ETV4 enrichment. DNA was quantified by qRT-PCR
835 using the ZRS 5'ST activity oligo set. Data are represented as mean \pm SEM of the fold
836 enrichment over nonspecific IgG recoveries from two independent experiments. (G)
837 Chromatin from 14Fp cells stably transfected with 3Xflag-*Gabpa* vector and an empty vector
838 as control was analysed by chromatin immunoprecipitation for GABP α and P300. DNA was
839 quantified by qRT-PCR using the ZRS 3'LR and 5'ST activity oligos sets. Average of
840 percentage of input \pm SEM from two independent experiments are plotted.

841 **Figure 6. ETV4 acts as a repressor via interactions with HDAC2**

842 (A) Quantitative RT-PCR to detect the mRNA levels of *Shh* (black box) in 14Fp cells
843 transfected with HDAC1 and HDAC2 siRNA either alone or combined and with nonspecific
844 siRNA as control. Data were collected after 18 hours of transfection. *Shh* levels were
845 evaluated relative to control and normalized to GAPDH levels. Data points represent the
846 average of triplicate determinations \pm SEM. (B) ChIP from two biological replicates using
847 the 14Fp cell line and anti- ETV4 and HDAC2 antibodies analysed by hybridizing to tiling
848 microarrays (FIG. 5-SUPL. 1B). Summary is presented using two different genomic regions,
849 the y axis is \log_2 for each ChIP/input DNA and the x axis represents a segment of DNA from
850 the microarray. The DNA region containing the ZRS is highlighted by the grey shading. As
851 controls, the whole of the *Shh* coding region plus promoter is shown. (C) 14Fp nuclear cell
852 extracts were analysed by immuno-precipitation with anti- ETV4 and IgG antibodies
853 followed by Western blot analysis with anti-HDAC2. (D) Quantitative RT-PCR to detect the
854 mRNA levels of *Shh* (black box) and *Etv4* (grey box) in 14Fp cells transiently transfected with

855 ETV4 siRNA (siETV4) or nonspecific siRNA (siCTR). Data points represent the average of
856 triplicate determinations +/- SEM. (E) Shown are results from ChIP analysis using anti-HDAC2
857 and ETV4 antibody after 24h of TSA treatment. Recovered DNA sequences were quantified
858 by qPCR using 5'ST oligo set. Average percentage of input and +/- SEM from two
859 independent experiments are plotted. The IgG did not give detectable signal.

860 **Figure 7. FGF signaling is responsible for priming the ZRS for local chromatin changes**
861 **mediated by ETS factors.**

862 Summary model showing how FGF signaling in the distal mesenchyme regulates the ZRS
863 poised state and that this allows the stepwise recruitment of transcriptional regulators to
864 the ZRS. FGF signaling has a dual fundamental role; firstly, as an activator it is responsible for
865 priming and maintaining the ZRS and secondly, as a repressor inducing the expression on
866 ETV4 which restricts the expression of the ZRS. ETV4 (red oval) interacts with HDAC2 (light
867 blue rectangle) to maintain the inactivity of the poised ZRS enhancer throughout the distal
868 mesenchyme, while GABP α (blue oval) acts within the ZPA domain to recruit p300 (yellow
869 rectangle), trigger H3K27 (orange circle) acetylation, and thereby activate *Shh* transcription.

870 **Figure 2-Figure supplement 1**

871 (A) RNA-seq analysis for 14Fp cell line and E11.5 distal limb bud. Fragments per kilobase per
872 million reads (FPKM+1) are plotted for a selected number of genes involved in limb
873 development. (B) RNA-seq analysis of E11.5 limb bud distal and proximal tissue and 14Fp
874 cell line. The relative expression FPKM+1 of *Hdacs* genes are represented in the chart. Two
875 biological replicates where analysed for each sample.

876 **Figure 2-Figure supplement 2**

877 (A) RT-PCR and quantitative (q) RT-PCR to detect the expression of *Shh* in E11.5 limb specific
878 cell line 14fp after treatment with TSA, FGF8, RA, and their combinations. The *Shh* levels
879 were evaluated relative to control and normalized to GAPDH levels. RT-PCR was normalised
880 to HGRPT. Data points represent the average of triplicate determinations +/- SEM. (B) RT-
881 PCR from 14Fp harvested 3, 6, 16 and 24 h after TSA treatment or 24h after DMSO
882 treatment as control (ctr). The limb specific markers *Hand2*, *Gremlin*, *Alx4* levels were
883 evaluated and normalised to HGPRT. (C) Immunofluorescence analysis of endogenous SHH
884 in 14Fp cells treated without and with TSA. Cells were stained with antibodies directed
885 against the SHH C-terminal and SHH N-terminal portion of the protein (ABCAM) 1/500,
886 nuclei were counterstained with DAPI. An Alexa Fluor® 488 (1/1000) (ThermoFisher) was
887 used as the secondary antibody.

888

889 **Figure 2-Figure supplement 3**

890 (A) Chromatin was prepared from E11.5 dissected limb buds (distal, proximal, anterior and
891 posterior) and from 14Fp cells 18, 24, 30 h after TSA treatment, 24h treatment with DMSO
892 was used as control (ctr). Shown are results from CHIP analysis using anti-H3K27ac antibody.
893 Enrichment of H3K27ac at the 5'ST region was detected by qPCR and represented as mean
894 of fold enrichment/background (IgG) ± SEM over three biological replicates. (B) Quantitative
895 (q) RT-PCR to detect the expression of *Shh* in embryonic cell lines at E11.5 from the limb
896 (14Fp) and the mandibule (MD) after TSA treatment. MDs do not express *Shh* in response to
897 the treatment. The *Shh* levels were evaluated relative to control and normalized to *Gapdh*
898 levels. (C) CHIP of 14Fp and MD cell line using antibodies to two different histone
899 modifications (H3K4me1 and H3K27Ac) analysed by qPCR. Low enrichment of H3K4me1

900 with the 3'LR oligos set was observed in MD in comparison to 14Fp and no enrichment of
901 H3K27Ac with the oligos set 5'ST was observed after TSA treatment. (D) Gel with three 3C
902 samples for the 4C experiment (ctr, 18h TSA and 24h TSA). Undigested and *HindIII* digested
903 DNA after cross linking was run on a 0.6% agarose gel and appears as a high molecular
904 weight smear running from roughly 12-4 Kb showing that they were all efficiently digested.
905 (E) Final 3C templates run as one tight band above 10kb in size on 0.6% agarose gel for the
906 ctr, 18h TSA and 24h TSA ligated samples. On the first lane as control a digested template is
907 loaded. (F) Final 3C libraries are redigested with *MluCI* and the products were run on a 1.2%
908 agarose gel appearing as smear between roughly 0.3 - 1kb. As control the ligated products
909 are run together with the samples.

910 **Figure 3-Figure supplement 1**

911 (A) Gel with four 3C samples (ctr and 24h TSA, in biological replicates). Cross-linked DNA
912 was either undigested or *HindIII* digested cross linked DNA was run on 0.6% agarose gel.
913 DNA appears as a high molecular weight smear running from roughly 12-4 Kb showing that
914 those were all efficiently digested. (B) Final 3C templates run as one tight band above 10kb
915 on a 0.6% agarose gel for the two biological replicates for samples either treated (+) or
916 untreated (-) with TSA. (C) 3C analysis of TSA (black lines) and no TSA treated 14Fp cell line
917 (red lines). The relative level of each ligation product (fragments -1 to 5) has been plotted
918 according to its distance (in kb) from the 5' end of the ZRS (see map below graphs). The bait
919 primer and the TaqMan probe are listed in TS2 which were designed according to the
920 position of the *HindIII* fragment at the 5'end of the ZRS. The mean of two biological
921 replicates is plotted. The data were normalized to an internal region of the ZRS included in
922 between two *HindIII* fragments (ZRS 3'LR CHIP, TS1). Below the graphs, the *HindIII* restriction

923 fragments are indicated. *Hind*III fragments are numbered from fragment -1 to 5. The
924 locations of the *Shh* gene and the promoter are indicated (black rectangles, black rectangle
925 with arrow). The position of the bait is also indicated (black circle). (D) 3C analysis of
926 posterior (black lines) and anterior (red lines) limb tissue dissected at E11.5. (E)
927 Representation of fold change of expressing *Shh* samples versus non expressing *Shh*
928 samples. TSA treated 14Fp over untreated 14Fp relative crosslinking frequencies are
929 represented with black bars and E11.5 posterior limb tissue over E11.5 anterior limb tissue
930 are represented with grey bars. The means \pm SEM are plotted.

931

932 **Figure 4-Figure supplement 1**

933 (A) Cell morphology of 14Fp was assessed after NIN and BGJ treatments by microscopy. Cells
934 were stained with 1X trypan blue and the number of blue nuclei assessed (red circles). No
935 differences were observed between the different treatments and the control. (B) Trypan
936 blue staining was performed on limb tissue dissected following a treatment of 4h with NIN
937 and analysed by microscopy. Represented are time 0, 4h media alone or 4h with NIN. No
938 differences were observed between the media alone or NIN treatment, (C) qRT-PCR to
939 detect the expression of *Dusp6* after 4 h of nintedanib (NIN), with or without supplement of
940 FGF8/10 for 6 h, and BGJ treatment. Data points represent the average of duplicate
941 determinations \pm SEM. (D) Chromatin from 14Fp was harvest after BGJ treatments and
942 ChIP for H3K4me1 was carried out. DNA was quantified by qRT-PCR using the ZRS 3'LR (D)
943 and *Shh* promoter oligos (E) as control. Data are represented as mean \pm SEM of the fold
944 enrichment over nonspecific IgG recoveries from two independent experiments. (F)
945 H3K4me1 ChIP of the proximal mesenchyme of E11.5 limb buds after 6h of exposure to

946 FGF8 and FGF10. Fold enrichment over nonspecific IgG recoveries and \pm SEM from 2
947 independent experiments are plotted. DNA was quantified by qRT-PCR using Shh promoter
948 oligos.

949 **Figure 5-Figure supplement 1**

950 (A) Map of the plasmid pSV40-Tet3G- pTRE3G-mCherry-Gabp α , showing in schematic
951 fashion the relative positions of notable features of the plasmid. (B) 14Fp nuclear cell
952 extracts stably transfected with 3Xflag-Gabp α and with an empty vector treated with or
953 without doxycycline were analysed by Western blot analysis with anti P300 and normalised
954 with anti H3. (C-D) Zoom out of the CHIP-chip in 14Fp cell line using H3K27Ac and H3K4me1
955 antibodies (C) and ETV4 and HDAC2 antibodies (D). Visualised is the region included
956 between Shh gene and Lmbr1 gene.

957

958 **Supplementary File 1. (A)** List of oligos used for qRT-PCR, q-PCR and CHIP. **(B)** List of oligos
959 used for 3C and 4C analysis.

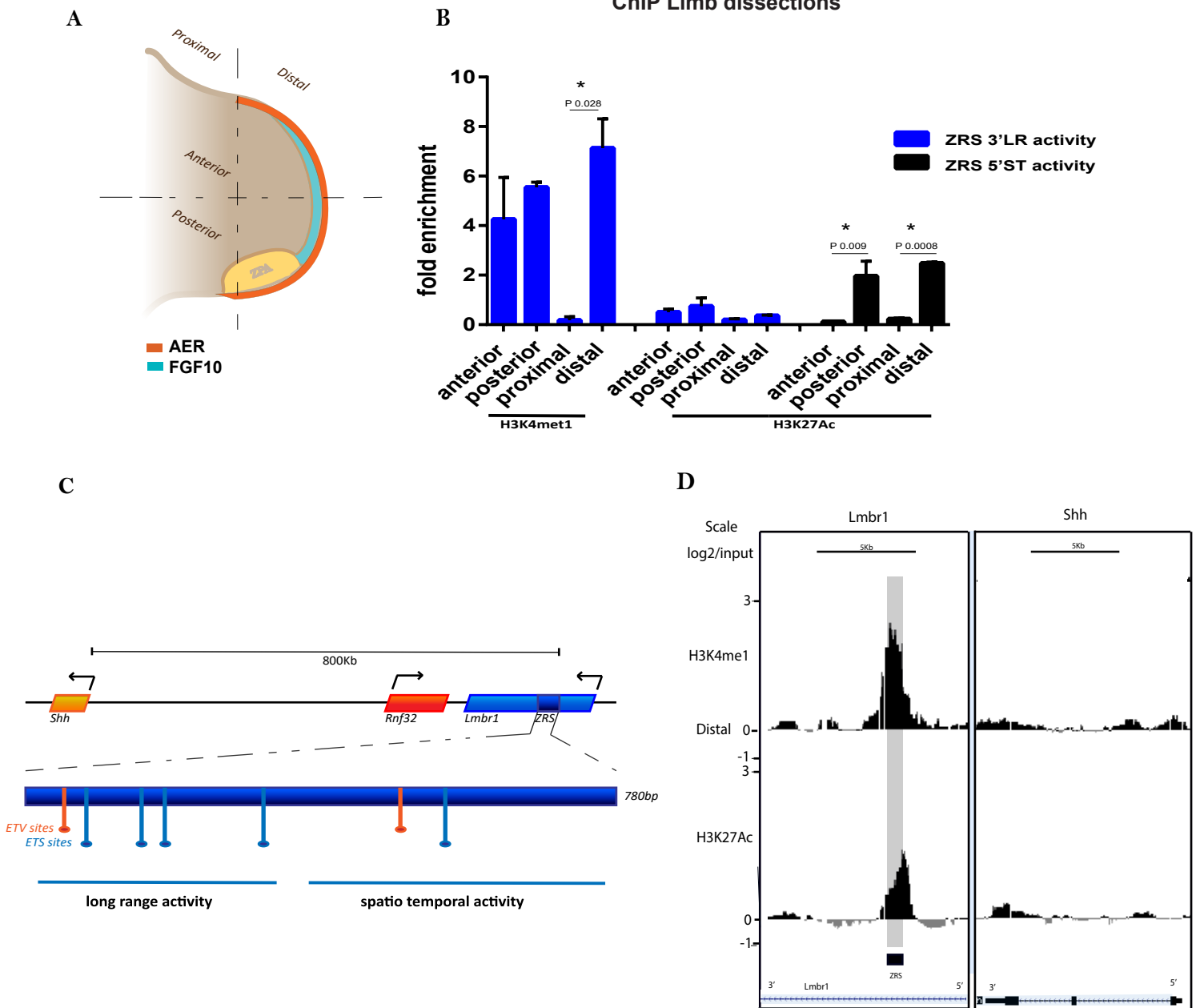
960

961

962

963

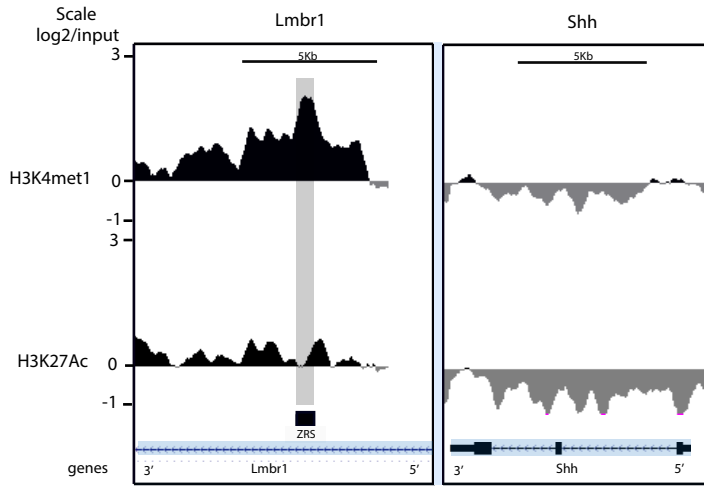
964



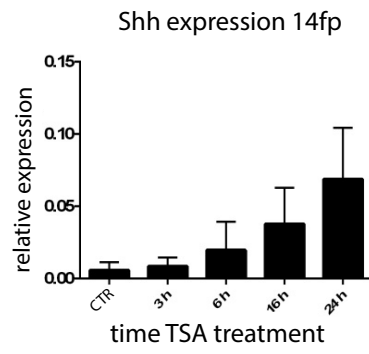
Peluso_Fig. 2

A

14fp

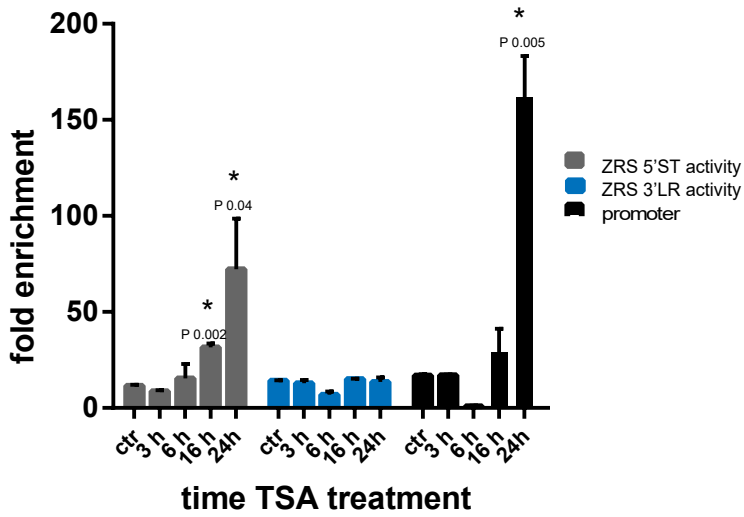


B



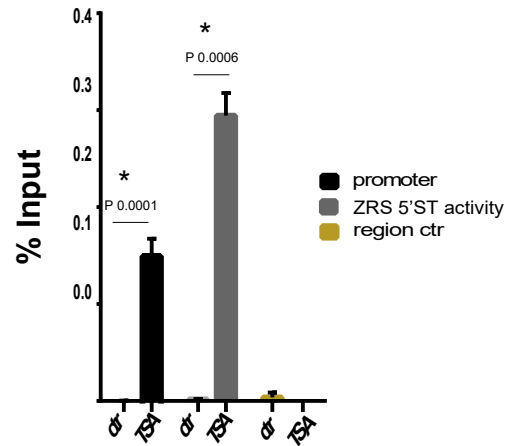
C

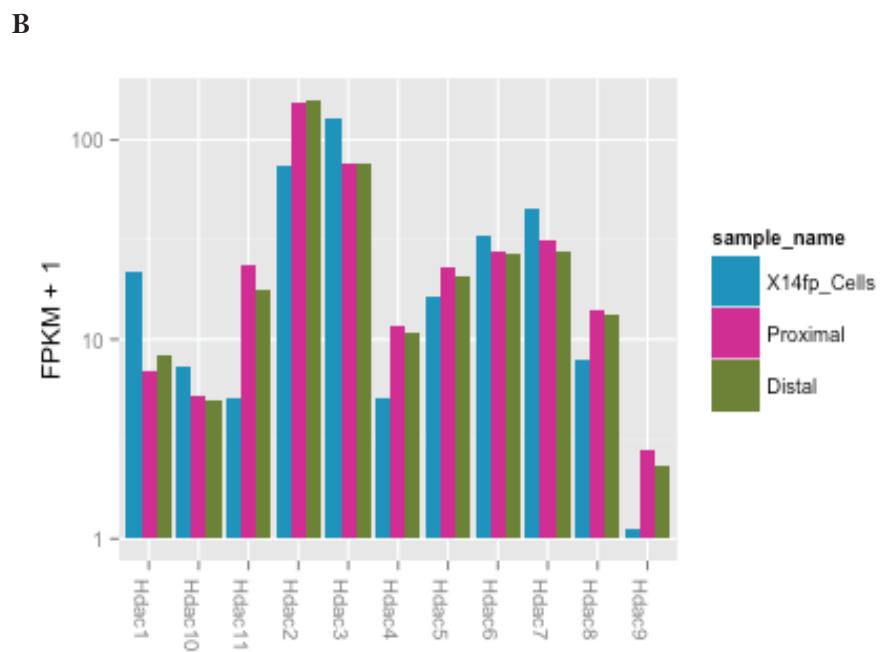
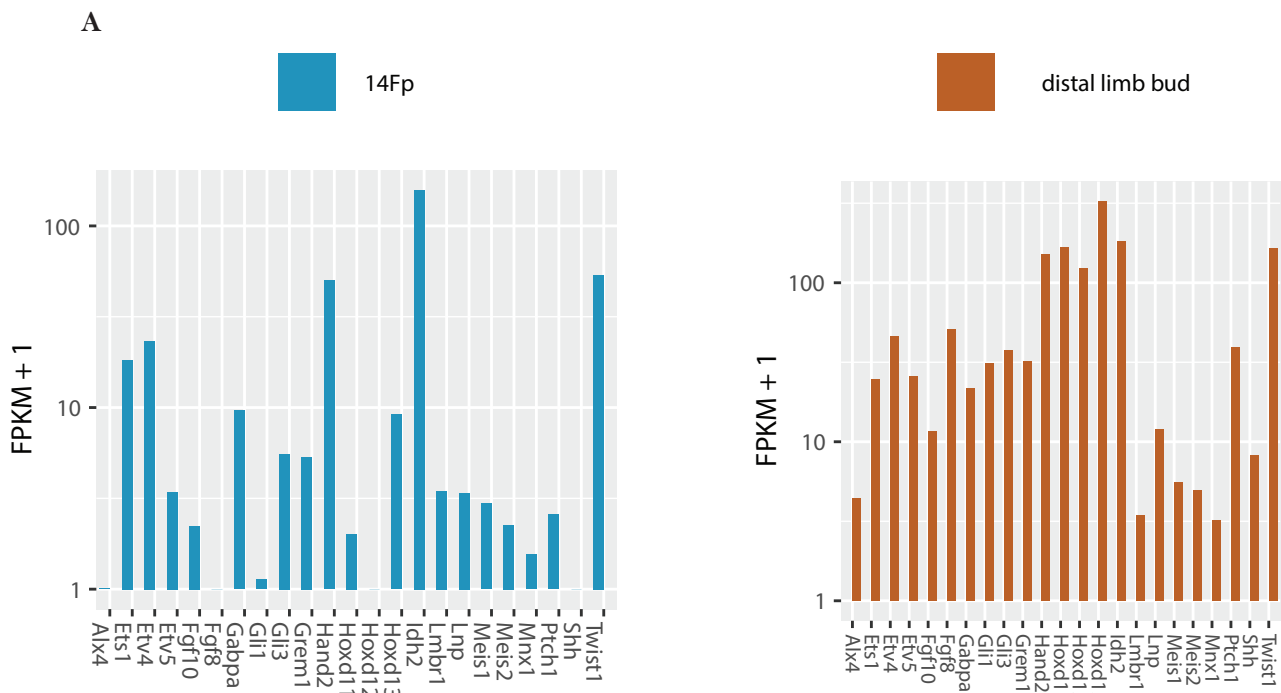
ChIP H3K27Ac 14Fp

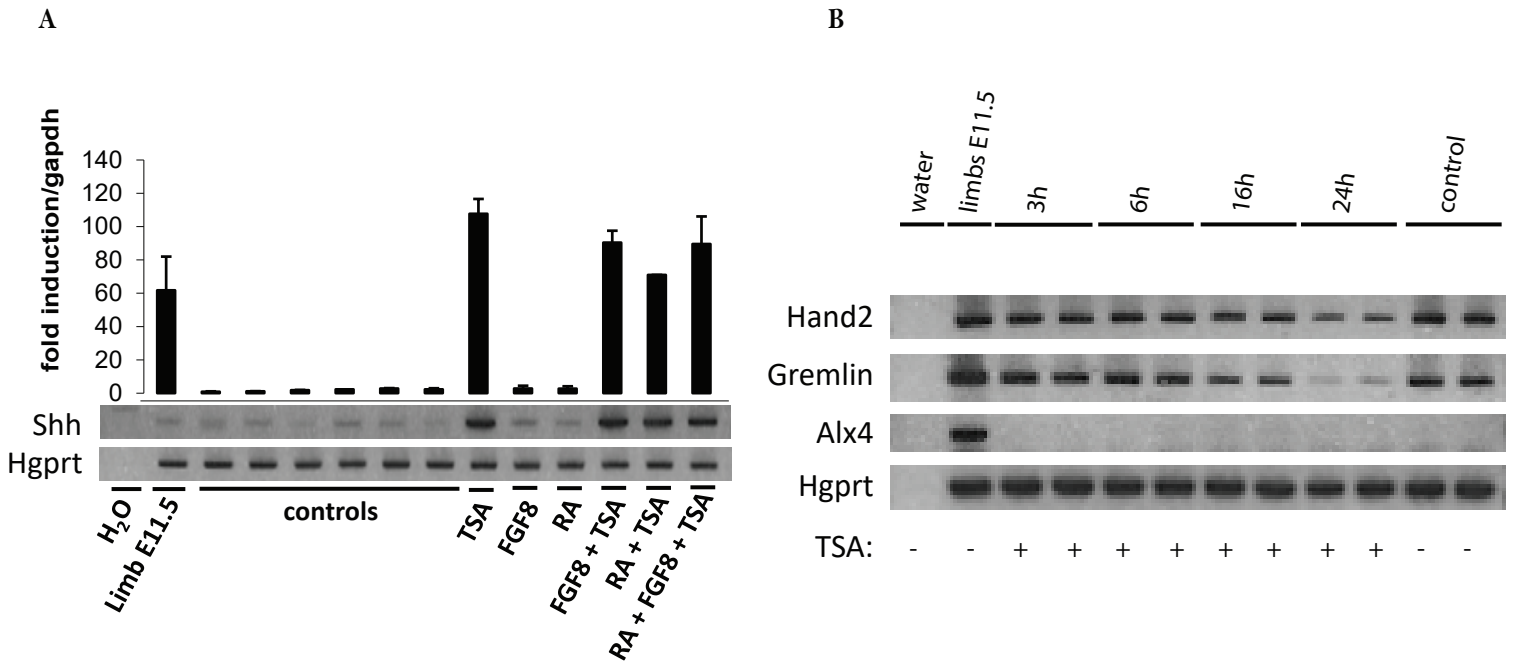


D

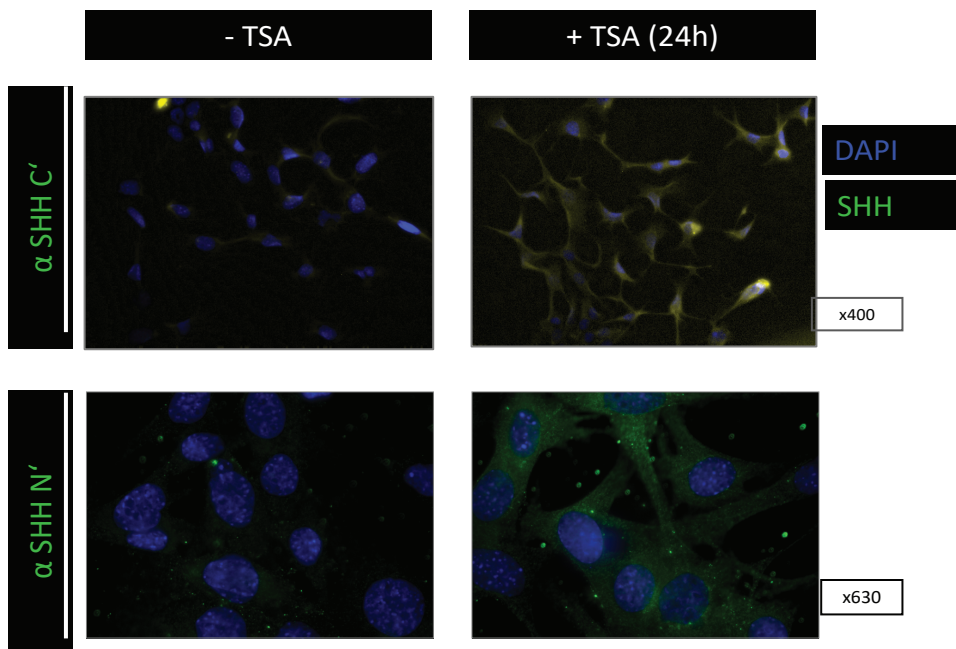
ChIP PolII 14Fp

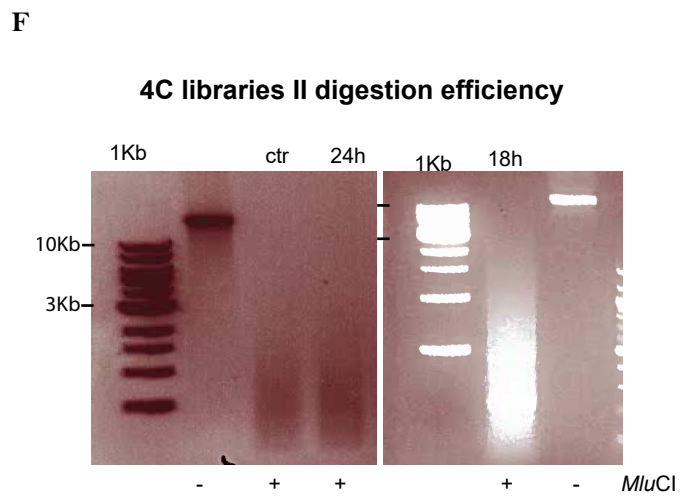
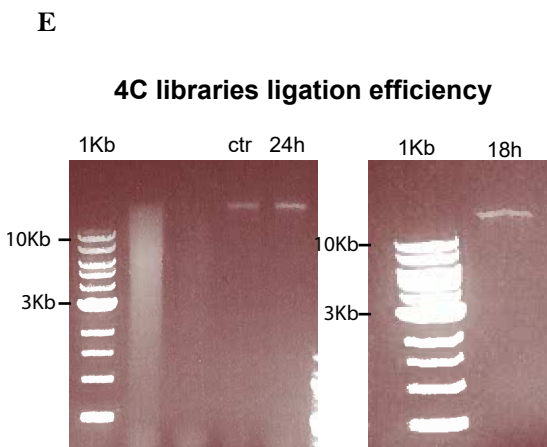
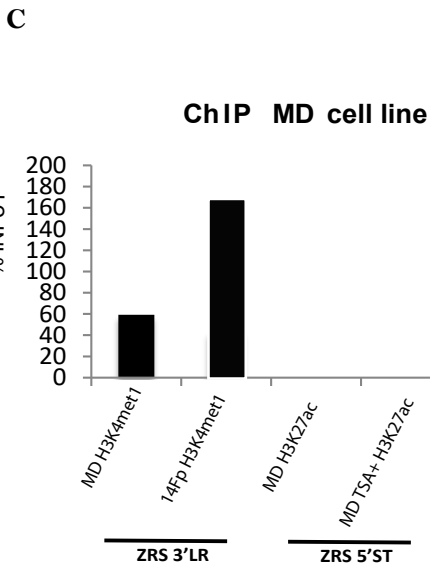
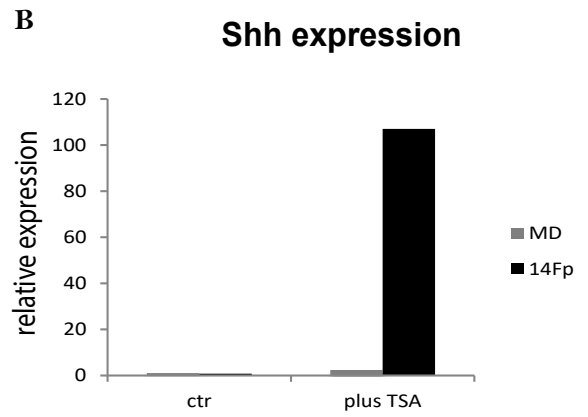
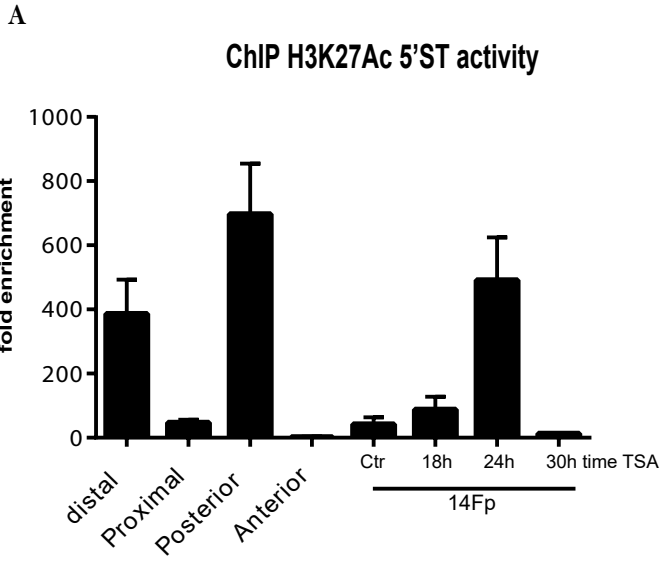


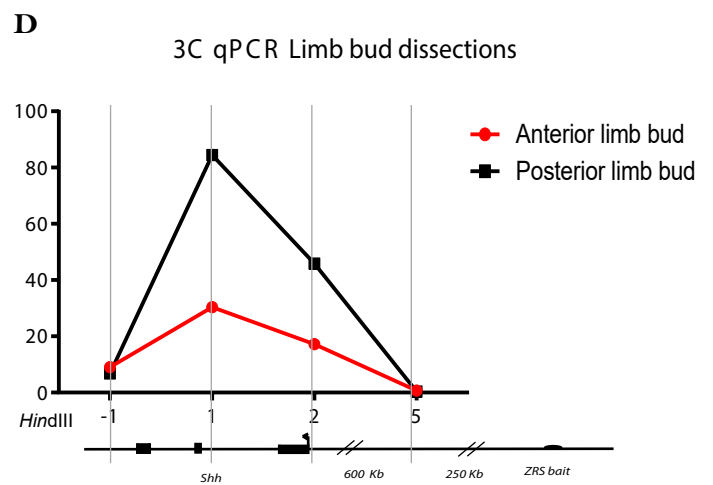
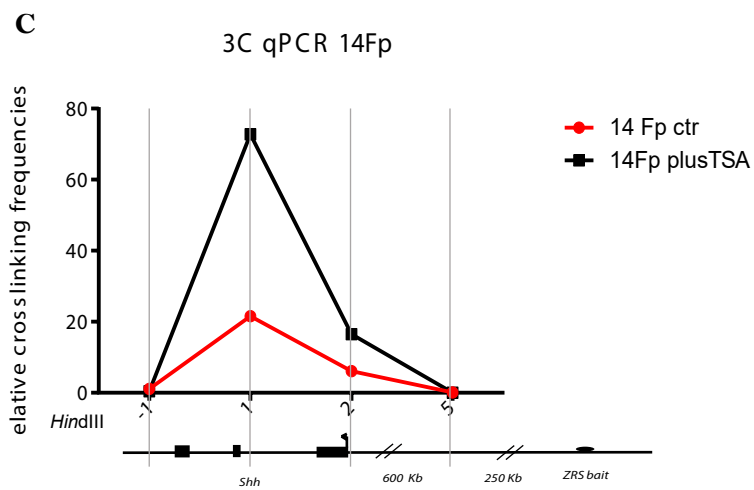
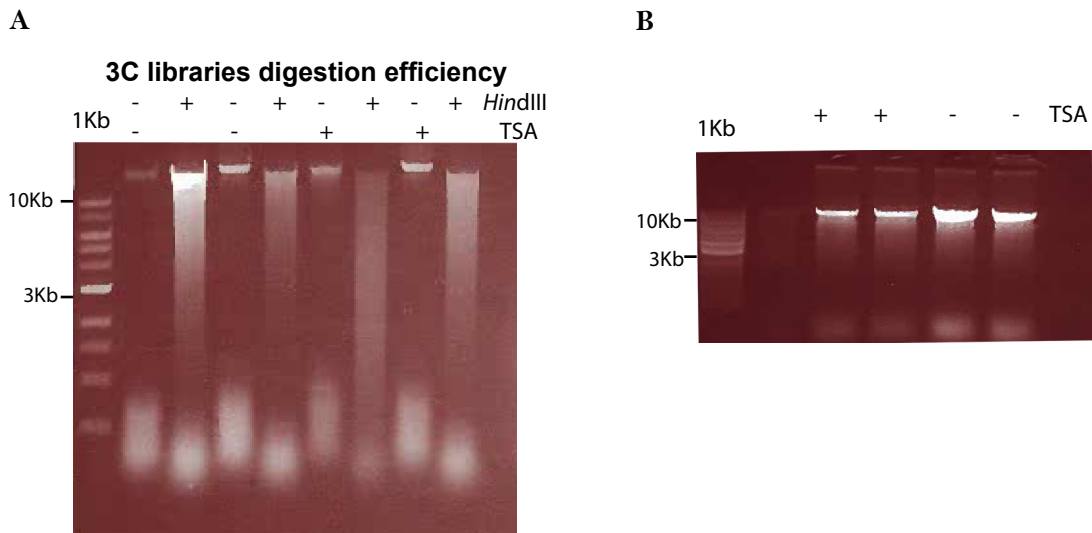




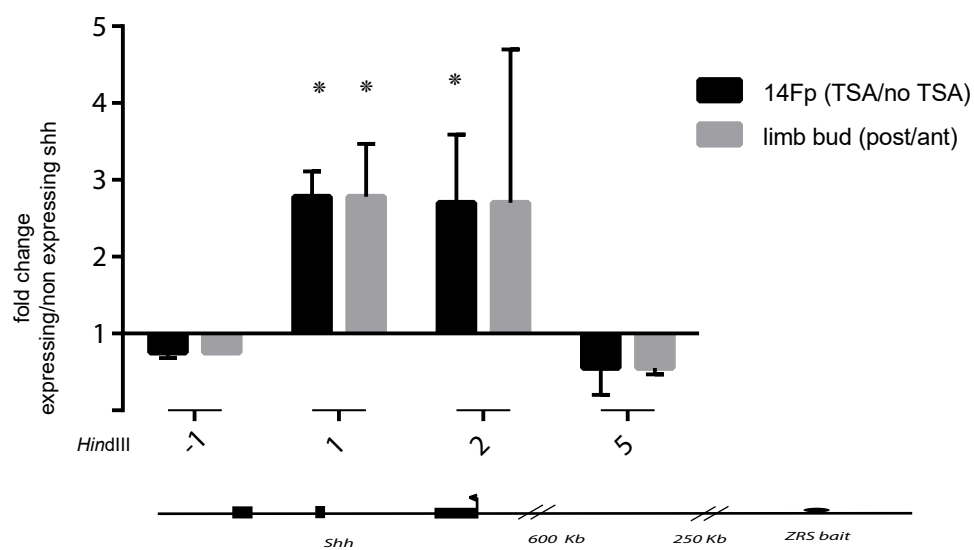
C





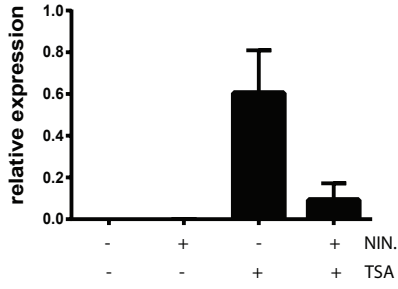


E Fold change relative cross linking frequencies



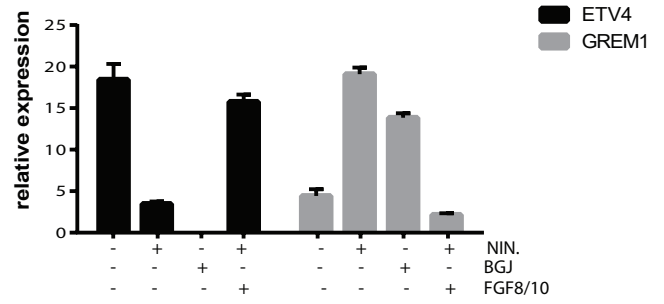
A

Shh expression 14Fp



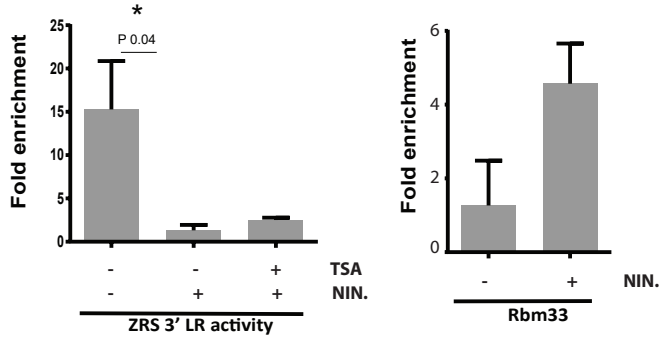
B

Etv4, Grem1 expression 14Fp



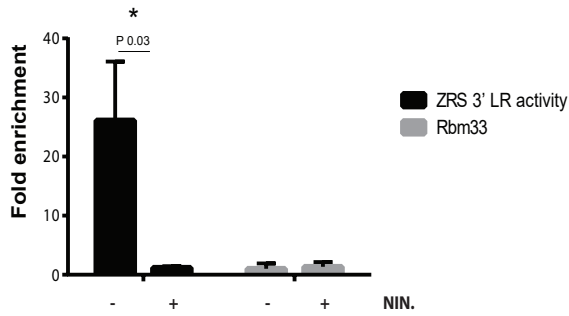
C

ChIP H3K4me1 14Fp



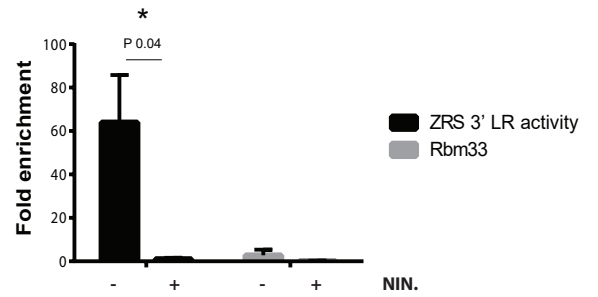
D

ChIP GABPa 14Fp



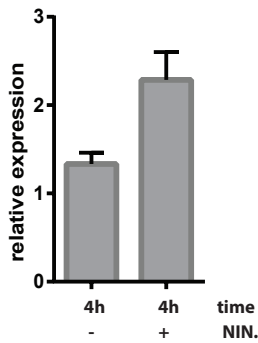
E

ChIP P300 14Fp



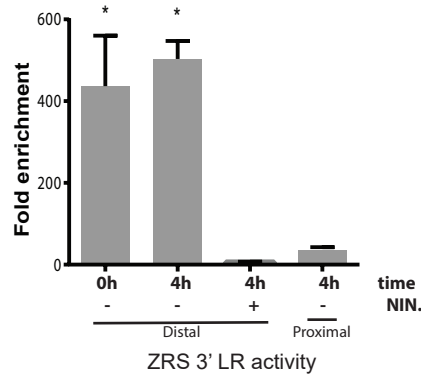
F

Grem1 expression distal limbs



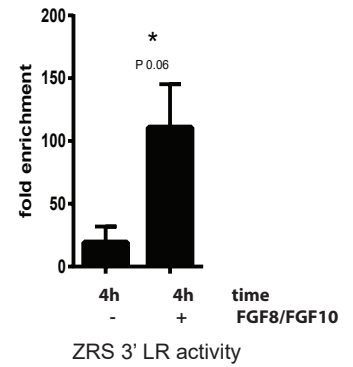
G

ChIP H3K4me1 distal limbs

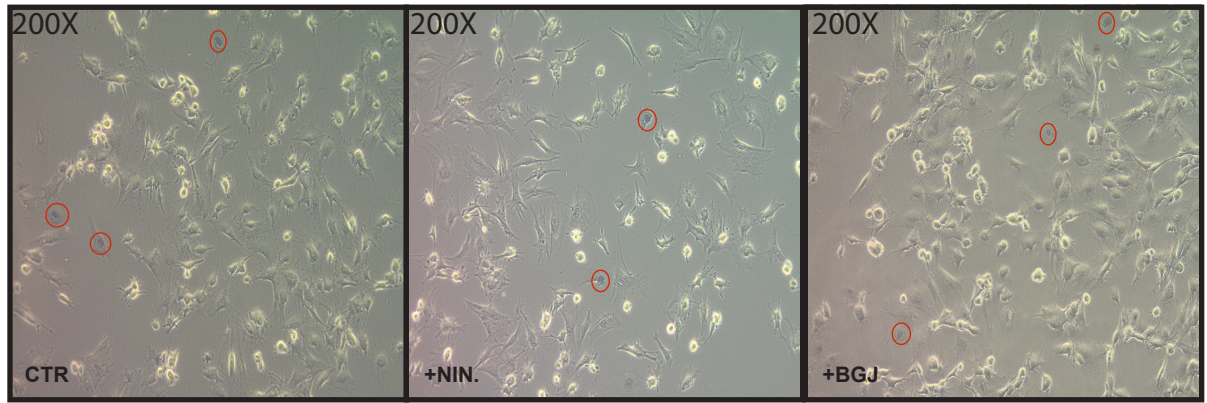


H

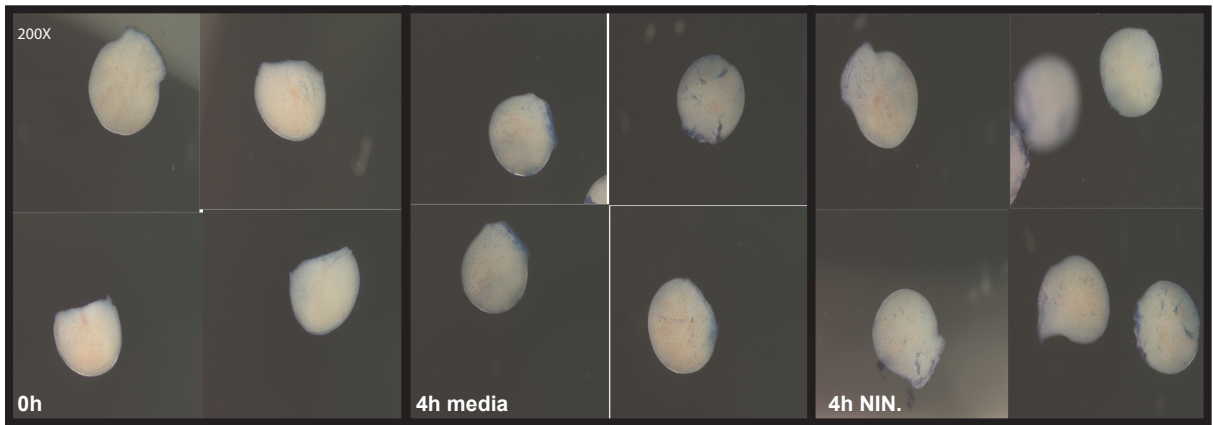
ChIP H3K4me1 proximal limbs



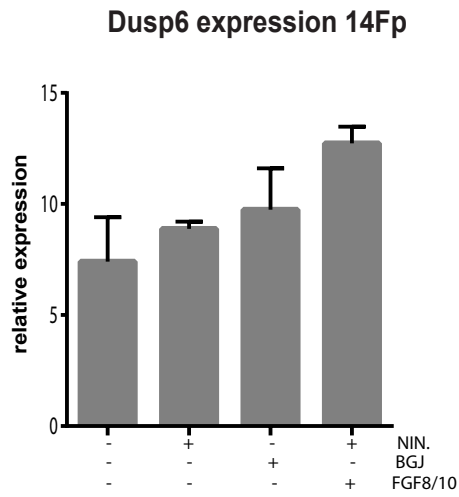
A



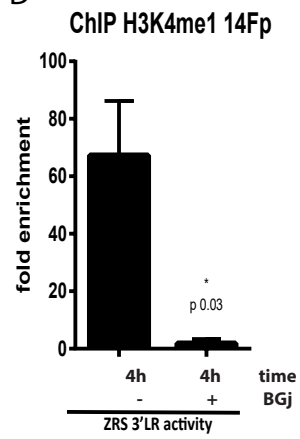
B



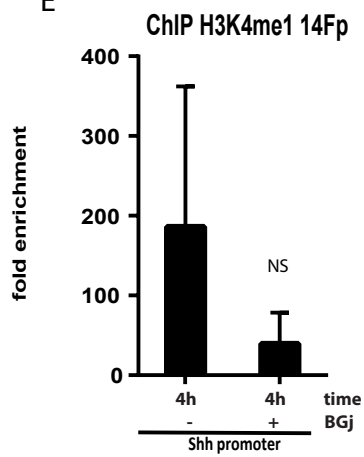
C



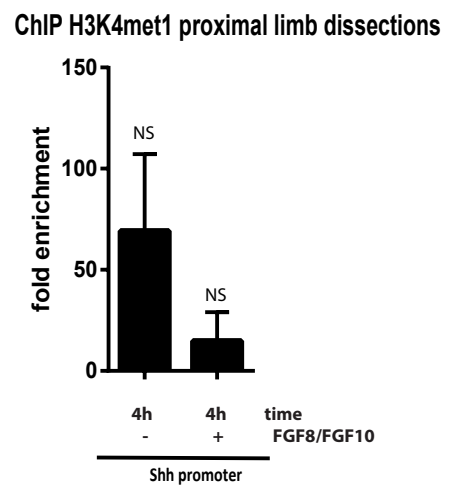
D



E

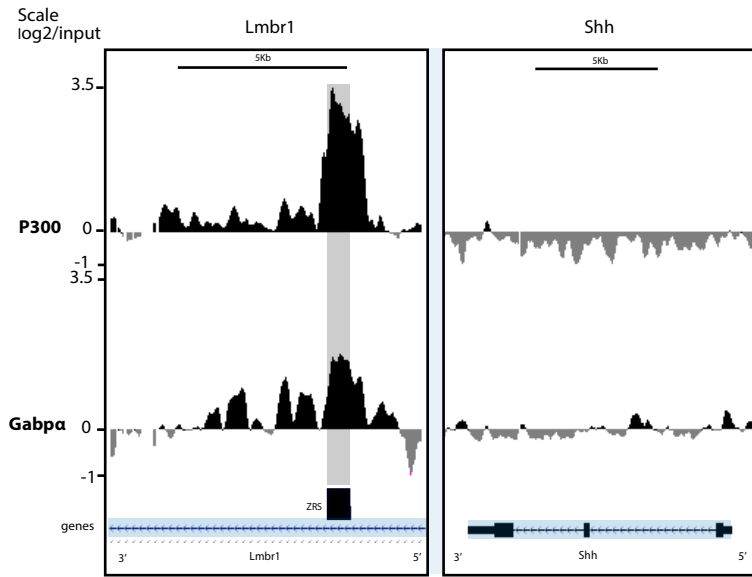


F

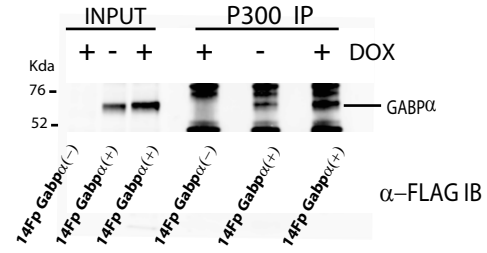


Peluso_Fig. 5

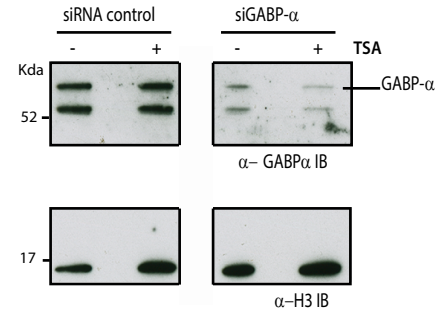
A



B

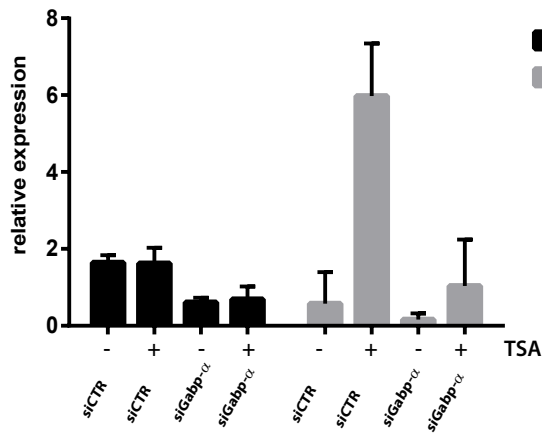


C

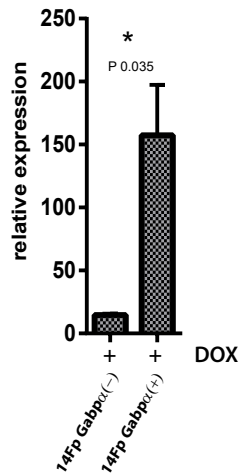


D

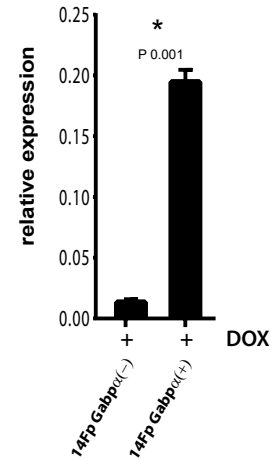
14fp Gabpα Knock down



Gabpα expression



Shh expression

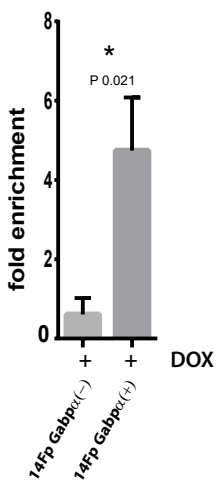


E

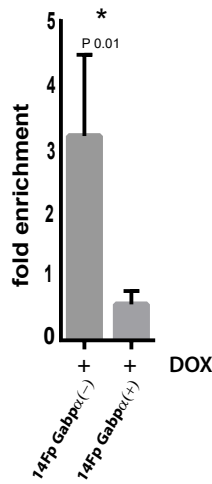
H

F

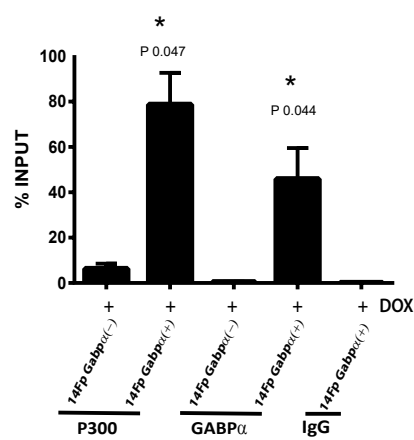
ChIP H3K27ac



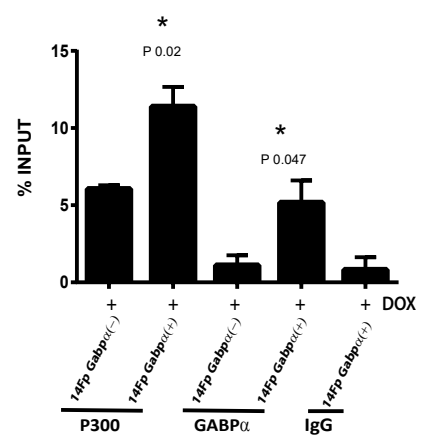
ChIP ETV4



ZRS 3'LR activity

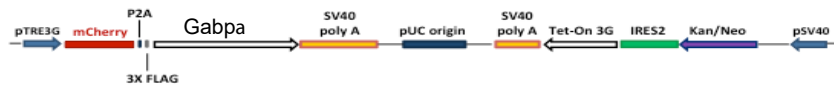


ZRS 5'ST activity

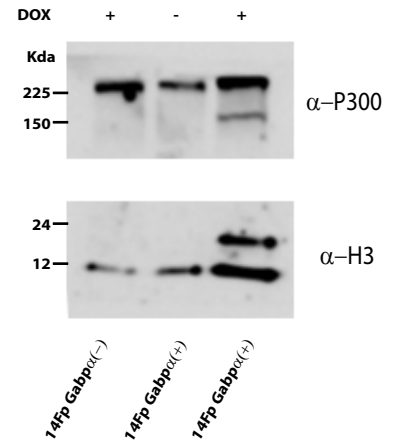


G

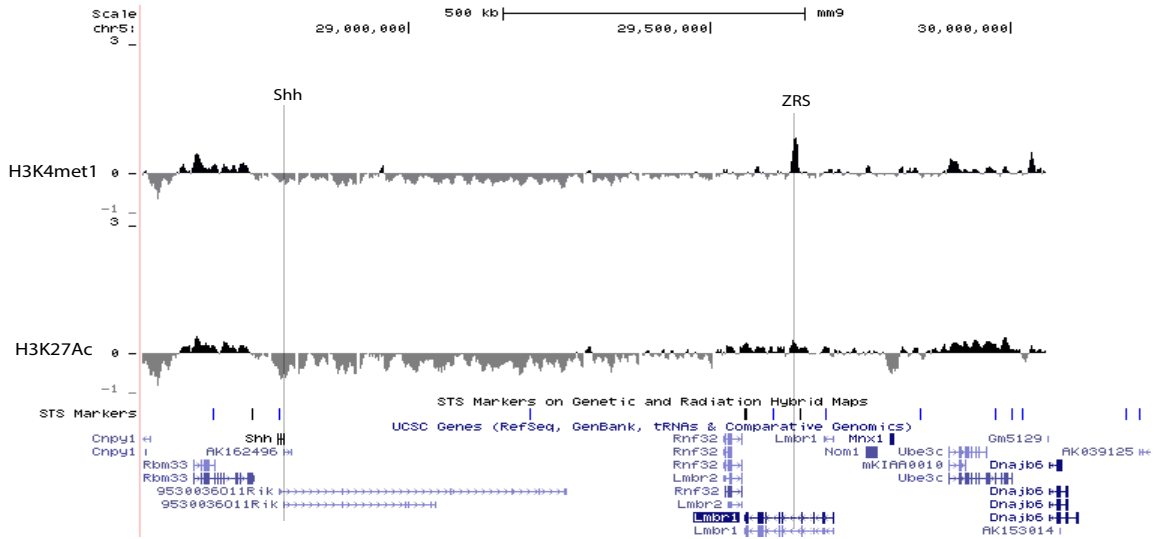
A



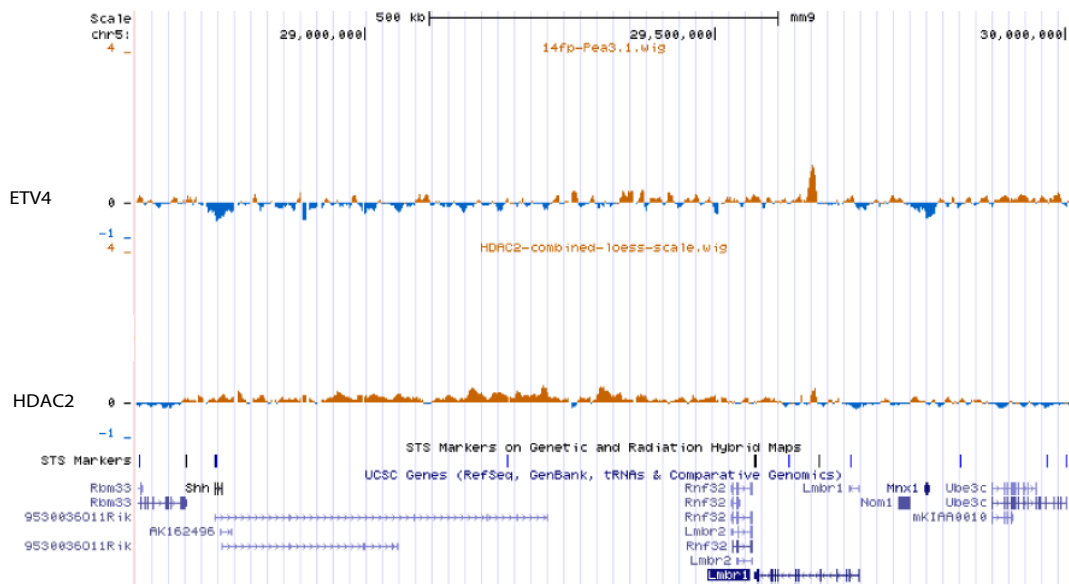
B



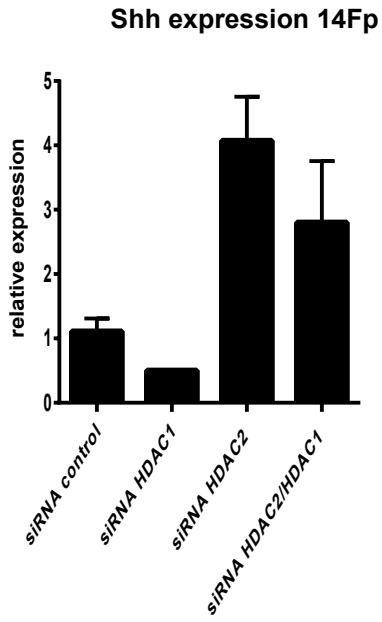
C



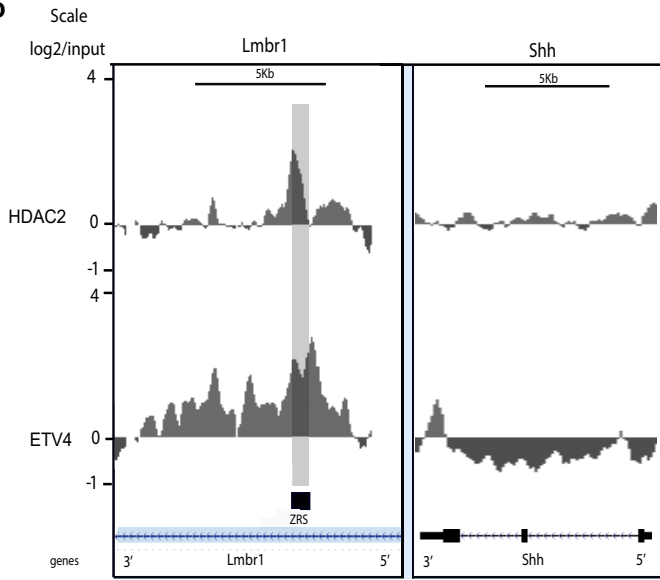
D



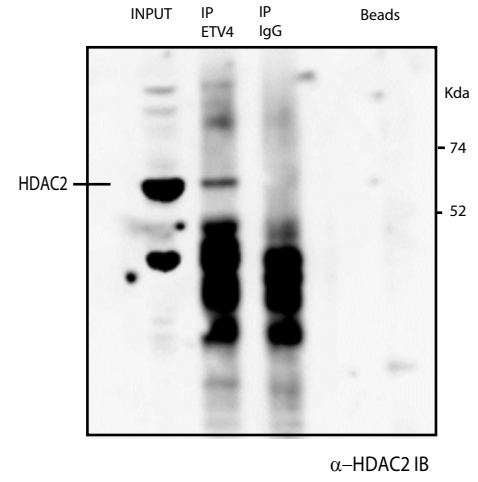
A



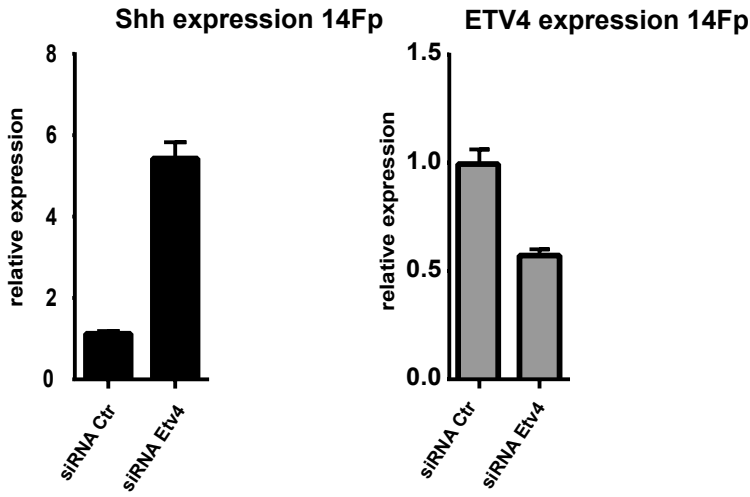
B



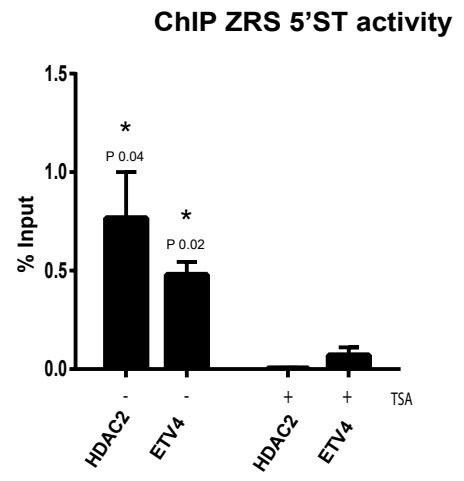
C



D



E



Peluso_Fig. 7

